Annu. Rev. Mater. Sci. 2000. 30:117–57

OPTICAL GENERATION AND CHARACTERIZATION OF ACOUSTIC WAVES IN THIN FILMS: Fundamentals and Applications

John A. Rogers
Bell Laboratories, Lucent Technologies, Murray Hill, New Jersey 07974; e-mail: jarogers@lucent.com

Alex A. Maznev and Matthew J. Banet
Philips Analytical, Natick, Massachusetts 01760

Keith A. Nelson
Department of Chemistry, Massachusetts Institute of Technology, Cambridge, Massachusetts 02138

Key Words mechanical properties, photoacoustics, ultrasonics, picosecond

■ **Abstract** The mechanical and acoustic properties of thin films and multilayer assemblies are important both for technological applications of these materials and for basic scientific studies of their physical behavior. Techniques that use optical methods to monitor acoustic waves stimulated in thin films with short pulsed lasers are useful for accurately and nondestructively characterizing the high frequency acoustic physics of these systems. This review briefly summarizes some of these techniques and focuses on a method known as impulsive stimulated thermal scattering or transient grating photoacoustics. It describes the most advanced experimental techniques for performing this measurement and outlines its application to the study of acoustic waveguide modes in a variety of thin films. These measurements, coupled with models for the physics of the modes, can be used to determine intrinsic mechanical properties of materials and structures that occur, for example, in microelectronics and high-frequency acoustic filters. This article summarizes a selected set of existing applications and concludes with an overview of future directions that include studies of the acoustics of complex microstructures such as microfluidic networks and synthetic phononic crystals.

INTRODUCTION

Advanced materials development is increasingly the driving force behind breakthroughs in a wide range of technologies. Thin films, in particular, play important roles in many devices due to their ability to enhance resistance to corrosion, wear,

and thermal breakdown. They are ubiquitous as conducting and dielectric elements in microelectronics and are often used as reflecting or polarizing elements in bulk and integrated optics. They have, in addition, many other applications in the aerospace, biotechnology, automotive, photographic, and magnetic disk industries. As the importance of advanced coatings and films increases, so does the demand for methods that can rapidly characterize them both during and after processing or deposition. Many conventional spectroscopic and scanning probe techniques can determine the chemistry, morphology, and electrical characteristics of thin films. It is generally difficult, however, to measure their mechanical properties. These quantities are often important because they can be either directly (e.g. for wear-resistant coatings or films for high-frequency acoustic devices) or indirectly (e.g. for process monitoring or in cases where mecchanical properties correlate to important device-related characteristics) relevant to the performance of these materials. The number of suitable measurement techniques is small, partly because interesting films can be thin (<0.1 μm is not unusual, and interlayer dielectrics thinner than $\sim$2 nm appear likely) and easily damaged (physical contact is typically unacceptable). They also often exist as coatings deposited at high temperatures or low pressures onto complex, non-planar objects. Scaled-down or otherwise modified versions of bulk testing techniques are currently the most common methods for examining the mechanical behavior of thin films (1–3). Emerging photoacoustic techniques based on short pulsed lasers provide attractive alternatives because they offer the possibility of fast, accurate, and noncontact evaluation with high spatial resolution. They also do not typically demand specially designed test structures.

There are, in general, three classes of approaches to high-frequency photoacoustic evaluation of thin films. In the first (Figure 1*A*) (4–7), a short pulse of light arrives at the surface of a sample and launches, through mild heating, a longitudinal acoustic pulse that propagates into the depth of the structure. Parts of this pulse are reflected at buried interfaces, such as those between films in a multilayer stack. A variably delayed probe pulse measures the time dependence of the optical reflectivity or the slope of the front surface of the sample in order to determine the time of arrival of the various acoustic echoes. Data from this type of experiment can be used to determine the longitudinal acoustic velocities when the thicknesses of the films are known, or to determine the thicknesses when the velocities are known. In a second method (Figure 1*B*) (8, 9), a cylindrically focused excitation pulse provides a broad-band line source for surface propagating waves that are measured by examining the changes in position, intensity, or phase of at least one probe beam that strikes the sample at a location spatially separated from the excitation region. The data in this case provide reliable measurement of surface acoustic waves velocities over a continuous range of acoustic wavelengths when the separation between the excitation and probing beams is known precisely. The methods shown in Figure 1 are similar in the sense that they both use an approach common to conventional acoustic techniques: There is a source of ultrasound, a propagation path, and a receiver or point of detection. They are also similar in their

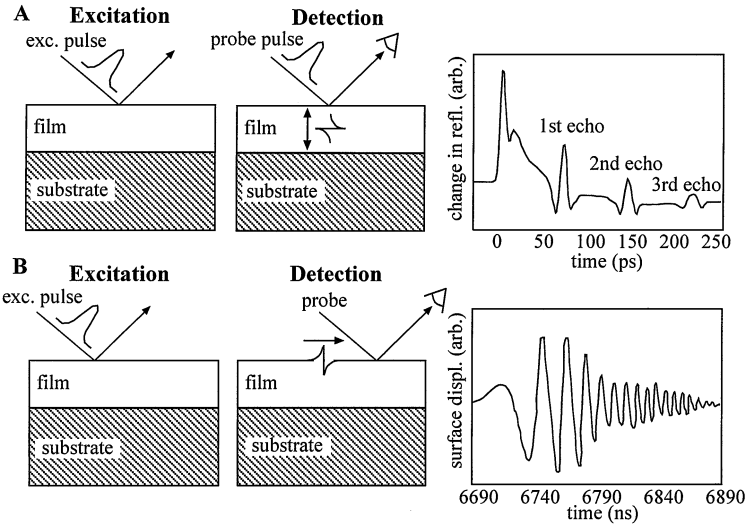

Figure 1 Schematic illustrations and typical data from two techniques for acoustic characterization of thin films using pulsed lasers. In the method shown in (*A*), an excitation pulse launches an acoustic disturbance that propagates into the depth of the film. A variably delayed probe pulse measures, in a point-by-point fashion, the time dependence of the change in reflectivity of the surface of the sample. The arrival of acoustic echoes reflected from buried interfaces changes this reflectivity slightly. In the technique shown in (*B*), a tightly focused excitation pulse generates surface acoustic waves. The propagation of these waves is monitored with a probe beam that is spatially separated from the excited region. The data in this case often consist of oscillations that reveal the variation in acoustic velocities over a range of wavelengths defined by the bandwidth of the excitation.

generation of an essentially single-cycle acoustic wavepacket that includes a wide range of wavevectors and corresponding frequencies.

The third method (Figure 2) (10–15), known as transient grating (TG) photoacoustics or impulsive stimulated thermal scattering (ISTS), relies on approaches that are more similar to light scattering techniques than to conventional acoustic methods. The TG technique uses the optical interference of two or more excitation pulses overlapped at the surface of a sample. Mild impulsive heating in a geometry defined by this interference pattern launches acoustic disturbances that consist of counter-propagating surface modes and bulk waves that travel into the interior of the sample. The time dependence of the diffraction of a probe beam that is usually overlapped with the excited region of the sample reveals the temporal behavior of the acoustic (and other) modes that contribute to the surface displacement, i.e. primarily surface acoustic modes. The detection of signal in this case is quite similar to surface Brillouin scattering (16), where a probe beam is diffracted by thermally excited, incoherent surface phonons. An important distinction is that in ISTS the signal from coherently excited surface phonons is relatively large and

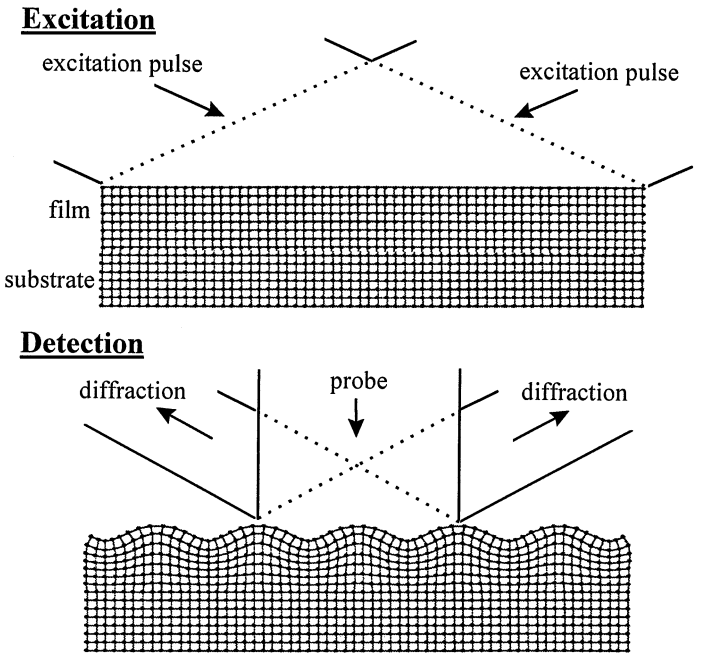

Figure 2 Spatial overlap of a pair of picosecond laser pulses at the surface of a sample generates mild impulsive heating in the spatial geometry of the optical interference pattern. This heating launches, through thermal expansion, coherent counter-propagating acoustic waves and thermal responses with wavevectors defined by the crossing angle and wavelength of the excitation pulses. Time-resolved measurement of the intensity of probe light diffracted from these motions reveals their temporal behavior.

can be detected and analyzed in the time domain (Figure 3). Also, although TG methods yield important acoustic information, it should be noted that they can be used to study thermal responses, dynamics of excited carriers, surface diffusion, and other processes (18–21).

This review summarizes our recent work in picosecond TG photoacoustic investigations of the behavior of thin liquid and solid films. Our aim is to provide an overview of the method, its capabilities, and certain important existing and future applications. We also hope to demonstrate that recent advances in experimental design have simplified the measurement dramatically, resulting in straightforward setup steps, very fast (∼1 s) data collection times, and even a commercial ISTS photoacoustic instrument whose operation requires no user adjustments of lasers or optics (22).

We begin with a brief description of the physics of the technique, and we outline the most advanced experimental approaches for performing the measurement. A discussion of the acoustic waveguide physics of thin films and multilayer assemblies provides a framework for interpreting the measurements. We illustrate how the data can be used to (*a*) determine isotropic and anisotropic elastic properties,

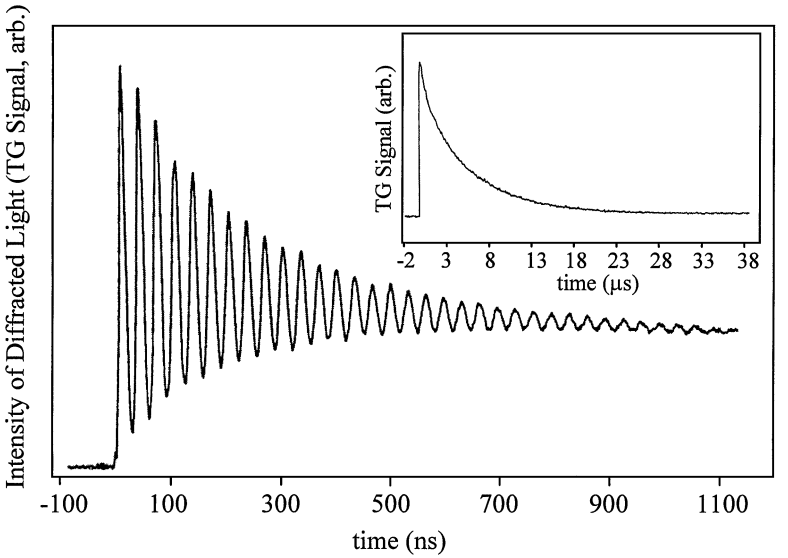

Figure 3 Temporal behavior of probe light diffracted by motions induced with picosecond laser pulses crossed at the surface of a thin (∼4.4 μm), free-standing polymer film. The onset of diffraction coincides with the arrival of the excitation pulses. The oscillations are associated with acoustic standing waves. The inset shows the signal on microsecond time scales; the slow decay is associated with the thermal component of the response. The frequencies and decay rates of the oscillations define the acoustic velocities and attenuation rates. The rate of decay of the thermal component can be used to determine the in- and out-of-plane thermal diffusivities.

(*b*) evaluate intrinsic stresses, (*c*) measure the thicknesses of transparent and opaque films, (*d*) identify and spatially map out film delaminations, and (*e*) profile depth-dependent film and substrate properties. Brief descriptions of TG analysis of films found in microelectronics and surface acoustic wave filters, and of dynamic changes in these systems, highlight some important existing applications. TG study of the high-frequency acoustics of optical fiber and planar microfluidic networks, subsurface defects and synthetic phononic crystals, and of acoustic motions excited with femtosecond pulses highlight some emerging future directions.

EXPERIMENTAL TECHNIQUES

Measurement Physics

The real-time transient grating photoacoustic or impulsive stimulated thermal scattering technique uses short (relative to the time-scale of the material response of interest) pulses of light from an excitation laser to stimulate acoustic motions in

a sample. The responses are usually measured with a continuous wave probe laser and fast detection electronics (15). Figure 2 schematically illustrates the mechanisms for excitation and detection in the simplest possible case. Here, two excitation pulses cross at an angle θ at the surface of a thin film on a substrate. The optical interference of these pulses produces a sinusoidal variation in intensity with a period Λ, given by

$$\Lambda = \frac{\lambda_e}{2\sin(\theta/2)}. \qquad 1.$$

If the excitation light (wavelength λ_e) is partially absorbed by the sample, then these pulses induce heating in the geometry of the optical interference pattern. The resulting spatially periodic thermal expansion launches coherent monochromatic counter-propagating surface acoustic waves with wavelength Λ and also launches acoustic responses propagating into the bulk of the sample. On a longer time scale, thermally induced strain slowly relaxes via thermal diffusion. The temporal nature of the resulting surface motions can be determined with each shot of the excitation laser by measuring the intensity of diffraction of a continuous wave probe laser with a fast detector and transient recorder.

Figure 3 shows typical data from a polymer film on a silicon substrate. The onset of diffraction coincides with the arrival of the excitation pulses at $t = 0$. The slow decay of signal is associated with thermal diffusion (inset of Figure 3); the oscillations are due to acoustic waves that propagate in the thin film. The frequencies and damping rates of the acoustic modes, along with the known acoustic wavelength, define the real and imaginary parts of the acoustic phase velocities. As discussed below, on a faster (picosecond) time scale it is also possible to resolve responses due to bulk longitudinal waves reflected from the film/substrate interface.

Data like those shown in Figure 3 yield the frequencies of acoustic motions at acoustic wavevectors defined by the optical interference pattern formed with the crossed excitation pulses. Although the frequencies themselves can be important (e.g. for surface acoustic wave filters and other applications), the intrinsic elastic properties of the films are often required. Determining these properties from the measured frequencies and the known wavevectors requires a detailed understanding of how acoustic waves propagate in layered systems. The physics can be complex, partly because thin films form acoustic waveguides for in-plane propagating modes (23, 24). Accurate determination of the elastic properties of the film demands accurate characterization of these modes, and typically requires a measurement of how their phase velocities vary with acoustic wavelength (i.e. a measurement of the acoustic dispersion). When two excitation pulses are used, adjusting the crossing angle changes the interference pattern fringe spacing and, therefore, the acoustic wavelength according to Equation 1. In the past, this adjustment involved physically moving mirrors, beamsplitters, and delay stages. An experimentally convenient and rapid means to adjust this angle, or a method to launch and monitor complex acoustic waveforms characterized by many wavevectors, is

essential for evaluating thin film systems or other samples (e.g. microstructures with feature sizes comparable to the acoustic wavelength) that show significant dispersion. A system that provides these and other features is described below.

Geometries for Excitation and Signal Collection

Figure 4 shows an experimental arrangement for exciting and detecting complex, wavelength-tunable acoustic waveforms (25, 26). It represents an extension of the traditional TG or ISTS approach. Excitation light passes through a beam-shaping optic that produces, from a single excitation pulse, a well-defined array of pulses. Imaging lenses recombine a selected set of these pulses at the surface of a sample. The pulses launch acoustic modes with wavevectors determined by the optical

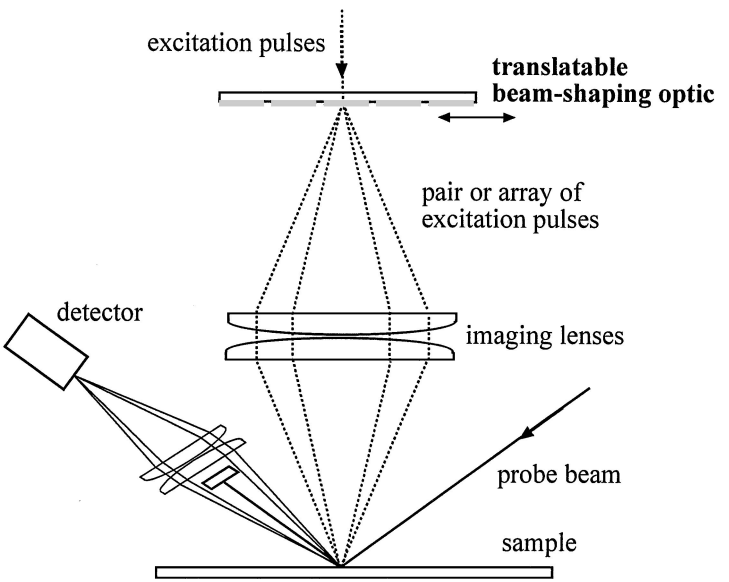

Figure 4 Optical arrangement for generating and delivering excitation pulses to the surface of a sample, and for monitoring the motions stimulated by these pulses. Excitation light passes through a beam-shaping optic that consists, for example, of a series of surface relief phase gratings with different periods. Each of these gratings splits a single excitation pulse into two or more pulses. A selected set of these pulses passes through an imaging lens pair and overlaps at the sample. The crossed pulses optically interfere and initiate material motions with wavevectors defined by the interference pattern. Light from a probe laser overlaps with the excited region of the sample; the material response diffracts a small fraction of this light. A lens pair collects the diffracted light and directs it to a fast avalanche photodiode. A transient digitizing oscilloscope records the output of the photodiode. Translation of different grating patterns on the beam-shaping optic into the beam path of the excitation laser provides a fast and simple way to adjust the wavevectors of the motions stimulated in the sample.

interference pattern that they form. The material response diffracts light from a continuous wave probe laser that is directed to the excited region of the sample. A lens pair collects the diffracted probe light and directs it to the surface of a fast photodetector; a fixed beam block removes undiffracted light. A transient recorder measures the time dependence of the diffracted light and, therefore, of the acoustic and thermal disturbances.

Translation of a beam-shaping optic designed with several spatially separated patterns (amplitude and/or phase-modulating regions) changes the excitation geometry. In the simplest case, this optic consists of a set of binary, square-wave surface relief phase gratings with different periods, optimized for diffraction at the wavelength of the excitation laser. A single pair of pulses ($\sim$80% of the incident light into the $+1$ and -1 diffracted orders) is produced by any one of these gratings (26). The period of the grating defines the angle of diffraction and, therefore, the angle of recombination (θ in equation 1) and the wavelength of the acoustic disturbance. Translating the optic causes the excitation light to pass through gratings with different periodicities; this translation easily changes the wavelength of the excited acoustic modes. Recording data at various positions of this optic reveals the acoustic dispersion of the sample. Figure 5 shows typical data. Each of these four traces was recorded from a thin film of NiP ($\sim$10 μm) on an aluminum substrate at different positions of the beam-shaping optic. Translation of the optic

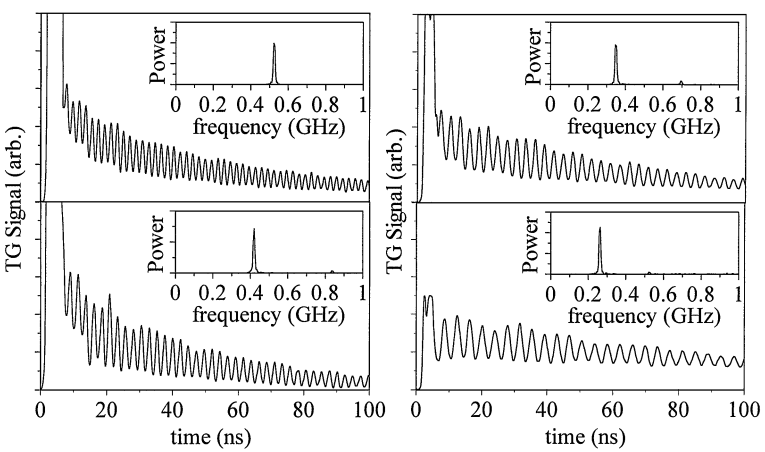

Figure 5 Typical data collected from the surface of a hard disk used for data storage (a $\sim$10 μm thick film of NiP on an aluminum substrate). The four traces were collected sequentially by translating a beam-shaping optic that consists of a series of spatially separated beam-splitting binary phase gratings (50% duty cycle, π phase shifting at $\sim$80% efficiency of the incident light into the $+1$ and -1 orders) with various periods. Each data sweep required $\sim$2 s to collect; adjustment of the beam-shaping optic required $\sim$1 s. Data from this type of experiment can be used to determine how the acoustic frequency varies with acoustic wavelength (i.e. the acoustic dispersion).

requires ∼1 s; it is the only mechanical adjustment needed to record these data. The periodicities of the gratings and the magnification of the imaging system determine the wavelengths of the acoustic modes. Fourier transformation of the data determines the acoustic frequency at each wavelength.

Complex Beam-Shaping Optics for Controlling the Pattern of Excitation

Data like those illustrated in Figure 5 determine the acoustic dispersion of the sample through a set of measurements performed in a serial fashion. Complex beam-shaping optics allow single-shot measurements of dispersion through excitation and detection of well-defined acoustic waveforms that are characterized by many wavevectors (25). In this case, the beam-shaping optic produces more than two excitation pulses. Optical interference of these pulses at the sample produces an acoustic waveform that generates several diffracted probe beams, all of which are simultaneously measured by the fast detector. Fourier transformation of the resulting data determines the frequencies of the various wavelength components of the acoustic disturbance. Figure 6 shows a scanning electron micrograph of a surface relief phase optic designed to split a single excitation pulse into an array of six pulses. Overlap of these pulses generates an acoustic response that, in this case, contains six different wavelengths. Data in Figure 6 illustrate the temporal behavior of this response; the power spectrum in the inset shows six peaks that correspond to the six wavelengths associated with the excitation pattern. This single measurement determines the acoustic dispersion of the structure.

Heterodyne Detection

The experimental system illustrated in Figure 4 not only provides the ability to launch tunable, complex acoustic waveforms, but also, with a slight modification, enables phase-stabilized optical heterodyne detection (26–28). Figure 7 illustrates a convenient experimental arrangement for this purpose (27). Passing collinear excitation and probing beams through a beam-shaping optic consisting of a grating that produces at least two diffracted orders yields a pair of excitation pulses and a pair of probing beams. One of these probing beams serves as a reference for heterodyne detection of signal generated by the other beam. The beam-shaping optic and the imaging lenses ensure that the reference and signal beams overlap spatially. Coherent optical interference yields a heterodyne signal, $M(t)$, that can be related to the amplitude of the electric field associated with diffraction from the stimulated material, $S_a(t)$, and the amplitude of the electric field of the reference beam E_r by

$$M(t) \propto \left| S_a(t) + E_r e^{i\phi} \right|^2, \qquad 2.$$

where ϕ is the difference in phase between the reference and diffracted light fields. When E_r is large, the cross term in Equation 2 dominates $M(t)$; this quantity can

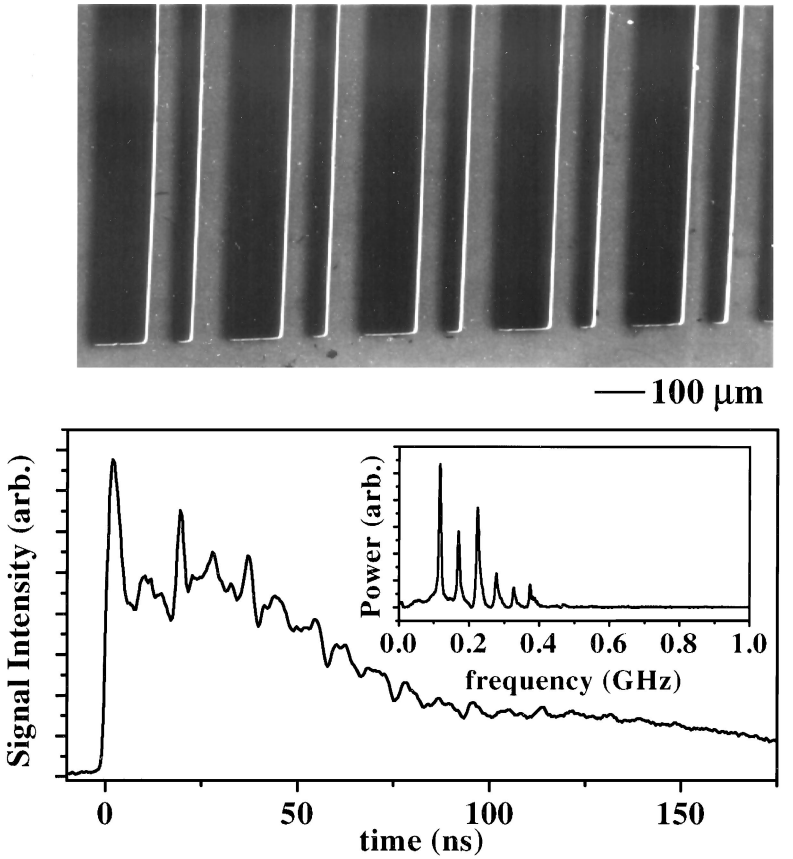

Figure 6 The *top frame* shows a scanning electron micrograph of a binary surface relief grating designed to produce from a single pulse an array of six excitation pulses with approximately equal intensities. Overlap of these pulses at the surface of a sample generates a complex acoustic waveform characterized by six wavevectors. The *bottom frame* demonstrates how collecting and measuring the probe light diffracted from this disturbance reveals its temporal evolution in real time. Fourier transformation of these data (inset, *bottom frame*) determines, in a single experiment, the acoustic frequencies at each of the acoustic wavevectors defined by the crossed excitation pulses. With this approach, the acoustic dispersion can be mapped out in a single experiment.

be much larger than $|S_a(t)|^2$, the signal that would be measured in the absence of the reference beam. Figure 8 shows data collected with and without a reference beam, and for two values of ϕ. It is clear that heterodyne detection increases the level of signal. This approach to detection can also be used to determine the phases of the various components of the material response $S_a(t)$ (27).

Another advantage of heterodyne detection is that it suppresses the effect of "parasitic heterodyning" caused by scattered light. Indeed, even when a distinct

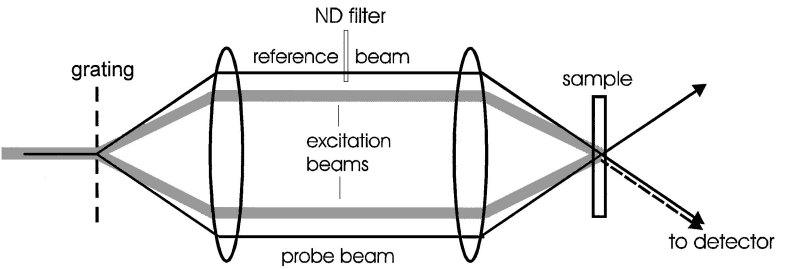

Figure 7 Experimental arrangement for transient grating photoacoustic measurements with heterodyne amplification. Collinear excitation and probing beams pass through an optic that diffracts these beams into at least two parts. The two excitation pulses launch a material response in a sample. One of the two probing beams serves as a reference beam for optical heterodyne amplification of signal generated by diffraction of the other beam. Overlap of the diffraction and the reference beam is guaranteed by the grating optic and the imaging lenses. For ease of illustration, the arrangement is shown in the transmission geometry. A similar setup is suitable for measurements in reflection mode.

reference beam does not exist, parastically scattered light will coherently interfere with the diffracted signal. If the scattered light intensity is comparable to that of the signal, the resulting heterodyne effect can be substantial. In this case, the phase ϕ can be adjusted to maximize the signal by simply translating the optic that produces the excitation beams, as illustrated in Figure 9 (25). This method enables

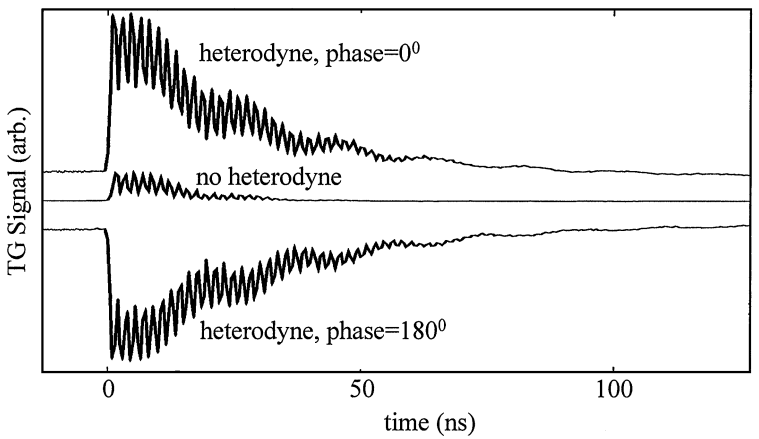

Figure 8 Typical data that show the effects of optical heterodyne detection of signals in transient grating experiments. Measurements were done on a 700 nm thick nickel film on silicon. The heterodyne signals are amplified by an amount determined by the intensity of the reference beam. The phase of this beam relative to the diffracted light also affects the measured signal.

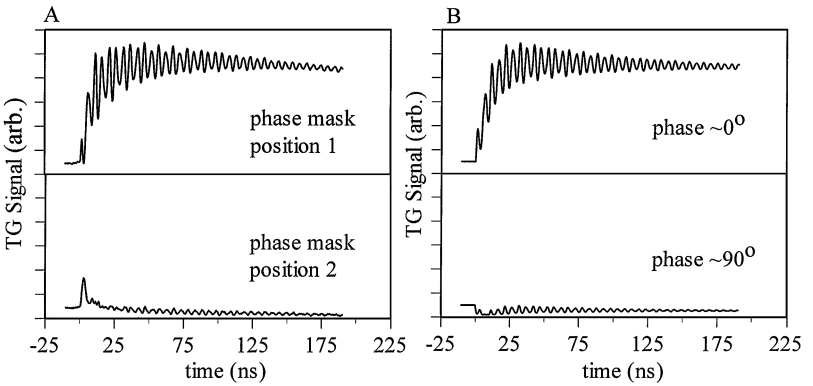

Figure 9 Measured (*A*) and simulated (*B*) data from a film (∼1 μm) of lead zirconium titanate on a film of platinum (∼100 nm) on silicon. This particular structure generates scattered light that overlaps with signal light and has an intensity comparable to that of the signal. The measured signal in this case is sensitive to the difference in phase of the scattered and signal light. These data illustrate the value of using beam-shaping optics to adjust and stabilize the phase of the signal (i.e. the phase of the excited modes) relative to that of the scattered light. By properly adjusting the position of the beam-shaping optic, it is possible to exploit parasitically scattered light to achieve heterodyne amplification of the signal. Without this capability, reliable measurement of samples that scatter light significantly is difficult or impossible.

measurements on highly scattering samples, although a more reliable approach is to use the heterodyne detection with a reference beam of much higher intensity than the scattered light, in which case the effect of the latter will be negligible.

Measurements on Picosecond Time Scales

In the experimental arrangement discussed above, detection electronics normally limit the frequency bandwidth of the measurements to about 1 GHz. There are several approaches for enabling measurements at faster time scales. One solution is to replace the fast photodiode normally used as a detector by an optical streak camera with temporal resolution down to 1 ps. As an example, Figure 10*A* shows a surface acoustic wave response at a frequency of ∼5 GHz.

With ultrashort excitation pulses and extended detection bandwidth, the achievable surface acoustic wave frequency is limited by the excitation wavelength and is in the 10 GHz range unless deep UV radiation or X-rays are used for excitation. The responses produced by the bulk longitudinal waves reflected from interfaces can, however, have frequency components much higher than 10 GHz. These responses have been measured using another approach to achieving high temporal resolution: femtosecond laser pulses were used for both excitation and, with a variable delay line, for probing (29). Figure 10*B* shows typical responses obtained from a metal film on Si. On a fast time scale, the data reveal picosecond responses due to the

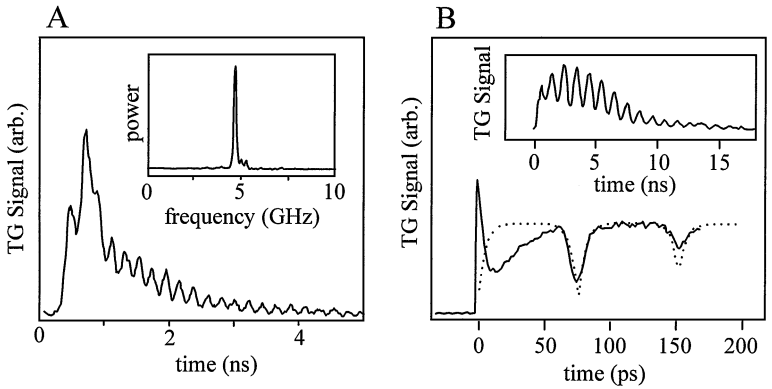

Figure 10 (*A*) shows transient grating (TG) signal from a film of titanium (215 nm thick) on a silicon substrate at a wavelength of 0.76 μm. These data were recorded with an optical streak-camera. (*B*) illustrates TG measurements of a thin ($\sim$250 nm) film of nickel on a silicon susbtrate performed using femtosecond pulses for excitation and detection. The inset shows oscillations that correspond to the types of planar acoustic waveguide modes that are the main focus of this article. The main frame shows that on picosecond time scales it is possible to observe, in the same experiment, acoustic echoes due to bulk longitudinal acoustic pulses bouncing between the free surface and film/substrate interface. The information contained in these data complement those determined from measurements of the surface propagating acoustic modes.

longitudinal acoustic pulse bouncing back and forth between the free surface and film/substrate interface. The duration of this pulse ($\sim$10 ps) is determined by the optical absorbtion depth in the metal at the excitation wavelength (4). On a slow (nanosecond) time scale, the signal is dominated by surface acoustic waves with wavelength Λ. These data demonstrate that the TG method has the combined power of the two photoacoustic techniques shown in Figure 1. It is capable of simultaneously measuring both out-of-plane acoustic echoes from the interfaces and in-plane surface acoustic modes.

Frequency Domain Detection

An alternative approach to signal detection that eliminates the bandwidth restrictions due to detection electronics is to analyze the spectrum of the diffracted probe beam with a scanning Fabry-Perot interferometer (30). This method exploits the fact that the diffracted probe light contains components spectrally shifted in frequency by an amount equal to the acoustic frequency. The spectra obtained in this way are quite similar to conventional surface Brillouin scattering spectra. However, the much higher amplitudes of the coherently excited surface acoustic waves in the TG technique allows a measurement time of $<$1 min compared with the several hours that can be required to collect a Brillouin spectrum of thermal

surface phonons (16). Disadvantages of frequency-domain detection compared with time-domain detection considered above include the inability to do single shot or real-time detection and the need to consider the often significant effects of the spectral resolution of the interferometer. Advantages include access to high acoustic frequencies without the need for high-bandwidth detection electronics and spectral isolation of signal, which confers relative insensitivity to parasitically scattered light associated with poor sample optical quality.

ACOUSTIC PHYSICS OF THIN FILMS

Guided Modes in Supported and Unsupported Films

Thin films, whether free standing or bound to substrates, are planar acoustic waveguides: In general they support multiple dispersive modes. The intrinsic acoustic properties and the densities of the materials that make up the waveguide, and any residual stresses in them, define the number of propagating modes, their velocities, and their dispersion. The normal modes of the waveguide can be computed by applying the appropriate equations of motion and boundary conditions to the system (23, 24). In the absence of nonlinear effects, displacements in each part of the waveguide must obey (31)

$$\frac{\partial^2 u_j}{\partial t^2} = \frac{c_{ijkl}}{\rho}\frac{\partial^2 u_k}{\partial x_i \partial x_l} + \frac{\partial}{\partial x_i}\left(\sigma_{ik}^{(r)}\frac{\partial u_j}{\partial x_k}\right) \qquad 3.$$

where u is the displacement, c is the stiffness tensor, ρ is the density, and $\sigma^{(r)}$ is the residual stress tensor. At free surfaces, the normal components of the stress tensor vanish. At interfaces between materials that are tightly bound to one another, the displacements and normal components of the stresses are continuous. These equations of motion and boundary conditions, along with the necessary stiffness tensors, densities, and residual stresses, can be used to compute the phase velocities of the various waveguide modes as a function of the magnitude and direction of the acoustic wavevector. For waveguides that include a single film with thickness h, it is possible to show that the velocities are functions only of the product of h and the acoustic wavevector (k).

Figure 11 shows the dispersion of the lowest ten waveguide modes that propagate in thin films of a typical unstressed, isotropic polymer bound to a silicon substrate and free standing (unsupported). In the former case (Figure 11*A*) the modes, known as Rayleigh or Sezawa modes, are strictly guided (i.e. displacements exponentially decay into the depth of the substrate) for velocities less than the transverse acoustic velocity in the substrate. When the acoustic wavelength is long compared with the film thickness (i.e. kh small), the effects of the film are small compared with those of the substrate. When $kh = 0$, only the lowest order mode is guided. Its velocity approaches that of the Rayleigh wave of the substrate in this limit. The Rayleigh wave involves acoustic motion localized to the surface

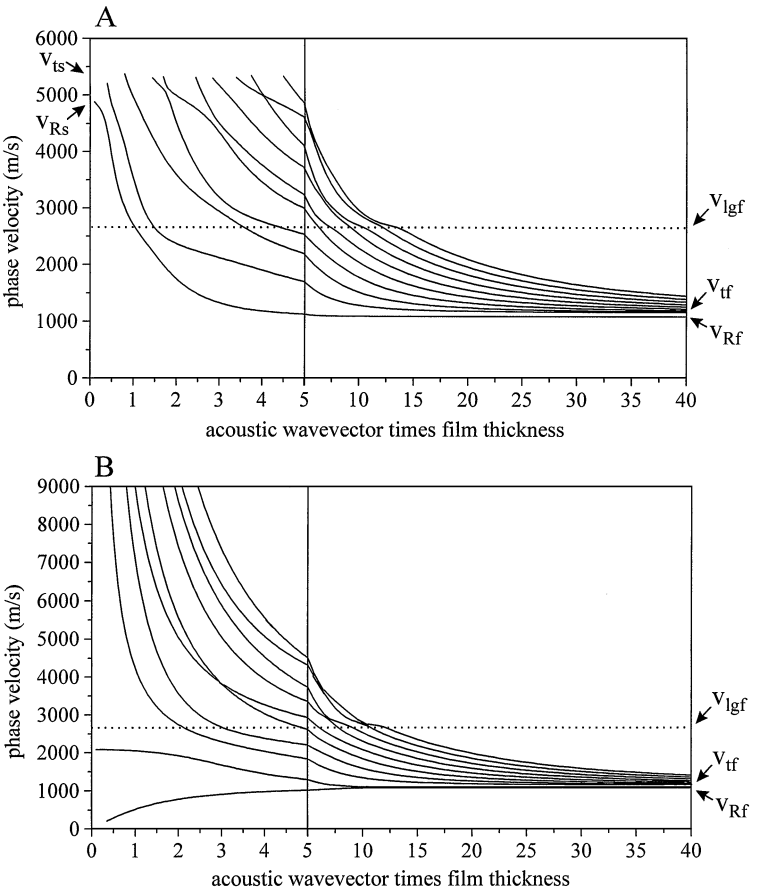

Figure 11 Calculated dispersion curves for the lowest ten acoustic waveguide modes in a typical polymer supported by a silicon substrate (*A*) and in a free-standing polymer film (*B*). In systems such as these, the velocities of the waveguide modes scale with the product of the acoustic wavevector *(k)* and the thickness *(h)* of the film. In both cases, the velocities approach intrinsic velocities of the film at large *kh*. (Note the change in the scale of the x axis at $kh = 5.0$.) All but the lowest order mode approaches the transverse velocity of the film (v_{tf}). The lowest order mode approaches the Rayleigh wave velocity (v_{Rf}). In the supported case (*A*), the lowest order mode approaches the Rayleigh wave velocity of the substrate (v_{Rf}) for small values of *kh*. All other modes are cut off at the transverse velocity of the substrate (v_{ts}). In the unsupported case (*B*), the velocity of the lowest order (drumhead) mode approaches zero for small *kh*. In this regime, the velocity of the second lowest order mode takes on a velocity slightly less than the longitudinal velocity of the film v_{lgf}.

of the structure. The decay with depth of displacements associated with this mode occurs on a length scale comparable to the acoustic wavelength. In the limit where the acoustic wavelength is short compared with the film thickness (i.e.*kh* large), the substrate has a small effect on the modes. In this regime, the mode velocities approach either the intrinsic transverse velocity of the film or, in the case of the lowest order mode, the film's Rayleigh wave velocity. The mode velocities and their variation between these limiting values are determined by the elastic properties of the film and substrate (e.g. Young's modulus and Poisson ratio, for isotropic systems), and densities of the film and substrate.

Like the supported system, the velocities of modes in an unsupported film (Figure 11*B*), known as Lamb modes, approach the intrinsic velocities of the film when the acoustic wavelength is short compared with the film thickness (i.e. *kh* large). There is no cutoff for guided modes because all of the acoustic energy is trapped in the film, which is surrounded by vacuum for these calculations. At small *kh*, the second lowest order mode involves primarily longitudinal displacements, and its velocity approaches a value slightly smaller than the intrinsic longitudinal velocity of the film. The velocity of the lowest order mode, which takes on the character of a drumhead or membrane mode at small *kh*, approaches zero when the residual stress is zero. In the presence of an isotropic, in-plane residual stress σ, this velocity approaches $(\sigma/\rho)^{1/2}$, the characteristic speed of waves on two-dimensional membranes. In polymers with stresses in the range of a few tens of MPa, the residual stress affects all modes other than the lowest unsupported mode at small *kh* by an amount that can be neglected in most cases. Figure 12 compares the calculated dispersion in unsupported polymer films with and without a residual stress of roughly 10 MPa.

Figure 13 shows grid distortion diagrams of the displacements associated with the three lowest order modes in the supported and unstressed, unsupported cases, at two values of *kh*. These diagrams clearly illustrate some of the effects discussed above. They also show that the number of nodes in the displacements through the thickness of the film increases with mode number. In the unsupported case, the in-plane displacements are either symmetric (e.g. second mode) or anti-symmetric (e.g. first and third modes) with respect to the center of the film. Each of these modes, and those in the supported case, involve in- and out-of-plane compressional and shearing motions; they are, as a result, sensitive to anisotropies in the in- and out-of-plane mechanical properties. The influence of the substrate and the differences between the spatial characters and mode velocities in the supported and unsupported cases increase with decreasing *kh*. This trend is particularly pronounced for the lowest order mode, whose velocity approaches zero or the substrate Rayleigh wave velocity in the unsupported or supported case, respectively.

It should be noted that in isotropic materials (and also in the symmetry planes of anisotropic materials), there exist two uncoupled families of waveguide modes: those polarized in the saggital (vertical) plane and termed Rayleigh or Lamb modes and those polarized in the horizontal plane (the plane of the surface) called Love

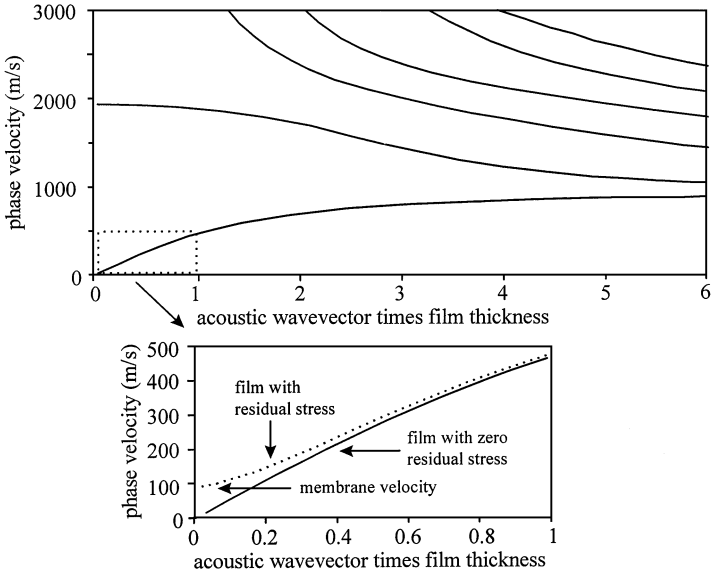

Figure 12 Computed dispersion for a thin free-standing polymer film with (dashed lines) and without (solid lines) residual stresses comparable to those found in typical polyimide films cured on silicon substrates (∼10 MPa). The calculations show that the stresses have small effects on all but the lowest order mode for this range of velocities and wavevectors. The frame on the bottom shows that as the product of the wavevector *(k)* and the film thickness *(h)* approaches zero, the effect of residual stress on the velocity of the lowest order mode becomes considerable. In fact, when $kh = 0$, the velocity of the lowest order mode in the stress-free film is zero. In the film that has residual stress, the velocity approaches that of a two-dimensional membrane and is proportional to the square root of the residual stress.

waves. These latter modes do not contribute to the surface displacement and, therefore, are not normally observed by the TG technique. The description presented above therefore focused only on vertically polarized modes.

In the general anisotropic case, the material displacement in an acoustic mode is no longer contained in either the vertical or the horizontal plane; the polarization pattern and phase velocity are both dependent on the propagation angle. These effects must be taken into account in analyzing measurements on anisotropic substrates such as silicon or lithium niobate. Figure 14*A* illustrates the computed variation in the phase velocity of the Rayleigh mode on the surface of a crystal of lithium niobate as a function of propagation angle. Figure 14*B* illustrates the angular dependence of the phase velocities of two lowest waveguide modes in a system composed of a thin polycrystalline film of titanium on a silicon substrate (001) (32). At 0° and 45° (high symmetry directions) the mode labeled R corresponds to the simple lowest order Rayleigh mode, and the mode labeled L is

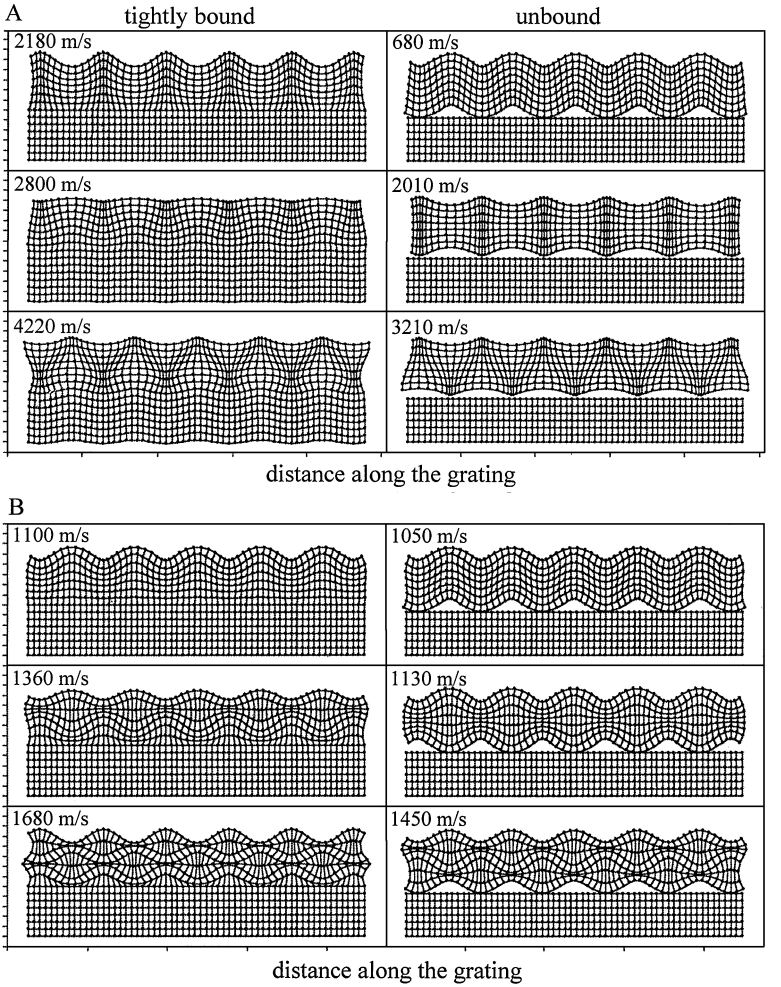

Figure 13 Grid distortion diagrams of the displacements of the lowest three guided acoustic modes for a typical polymer film tightly bound to a silicon substrate (*left frames*), and for a polymer film completely decoupled from the substrate (*right frames;* equivalent to free-standing film). (*A*) shows the nature of the modes when the product of the acoustic wavevector *(k)* and the film thickness *(h)* is equal to 1.5. (*B*) shows the same modes at $kh = 8.0$. In general, high order modes involve complex displacements with multiple modes in displacement through the depth of the film. At small *kh*, the coupling of the film to the substrate causes large differences between the nature (e.g. spatial characters and frequencies) of the modes in the bound and unbound systems. For large *kh*, the differences in the patterns of displacement near the surface of the film and in the phase velocities diminish.

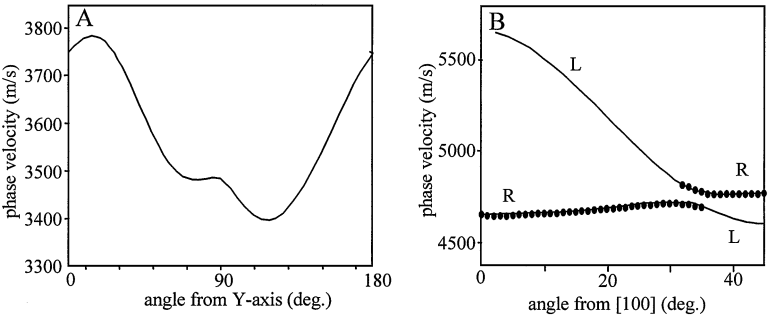

Figure 14 (*A*) shows the calculated dependence of the phase velocity of the Rayleigh mode on the X-cut surface of a crystal of lithium niobate as a function of propagation angle relative to the Y-axis. (*B*) shows angular dependence of the acoustic phase velocities of the lowest two modes in a film of titanium on silicon (001) calculated (solid line) and measured by TG technique (solid ovals) when the product of the acoustic wavevector and the film thickness is 0.19. The two modes correspond to uncoupled Rayleigh and Love modes at 0° and 45°. The mode with the largest surface ripple appears most strongly in the TG signal.

the Love mode. At other angles, these modes have mixed character. Below 35°, the lowest mode is predominantly a Rayleigh type mode, whereas the faster mode is predominantly Love type. At 35° there is an avoided crossing at which the modes exchange character. The TG technique is most sensitive to Rayleigh-type modes, which can limit the range over which the two modes can be probed easily. Although these and other effects can complicate the analysis of TG data, the additional information can increase the accuracy and precision of thin film properties extracted from these data.

Transient Grating Measurements of Guided Mode Acoustics in Thin Films

Transient grating experiments on thin films directly reveal nearly all of the important aspects of acoustic waveguide physics outlined in the previous section.

Delamination At a simple level, TG measurements at acoustic wavelengths much larger than the film thickness can be used to exploit the dramatic differences between the velocities of modes in unsupported and supported films for identifying, in a noncontacting, nondestructive manner, the presence of film delaminations or disbonds (33). Figure 15 shows, for example, TG signal collected using a pair of strongly absorbed ultraviolet excitation pulses from two regions of a single sample of a spin-coated polymer film on a silicon wafer. The data in the bottom frame were collected from a region of the sample from which the silicon was etched away. The dominant frequency corresponds to the lowest order Lamb mode, which has a low phase velocity in this small *kh* regime. The upper

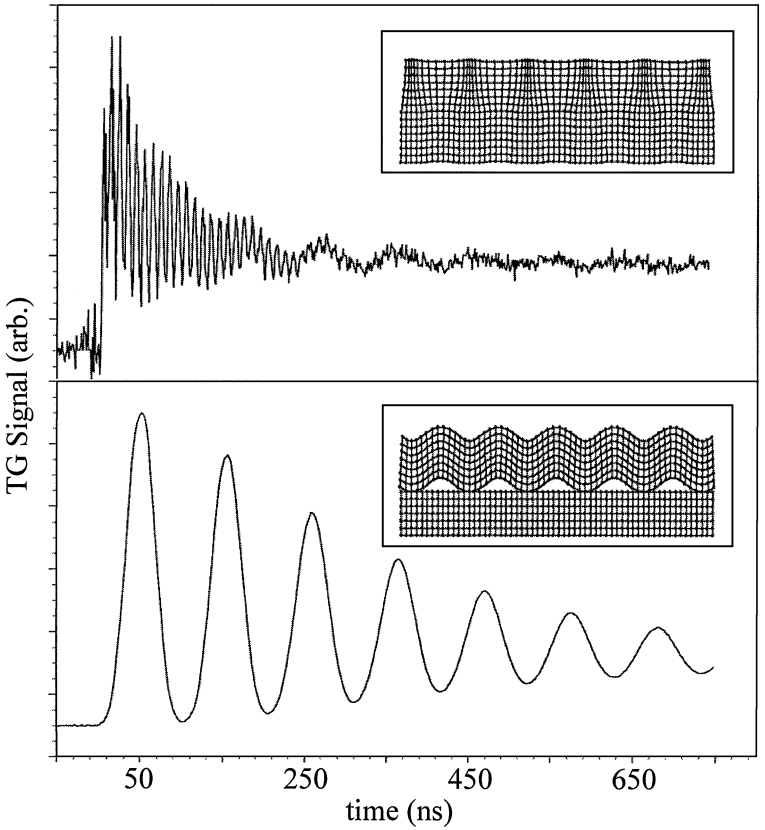

Figure 15 Data collected at a single acoustic wavelength (22.25 μm) from two regions of a spin-cast polyimide film (thickness 2.16 μm) on silicon. The *top frame* shows data from a part of the sample where the film is tightly bound to the substrate. The frequency of the acoustic mode is high because the phase velocity approaches the Rayleigh wave velocity of the silicon substrate when the product of the wavevector and thickness is small. The data in the *bottom frame* were collected at the same acoustic wavelength from a region of the sample that was not bound to the substrate (i.e. at the location of a disbond). The lowest order anti-symmetric Lamb mode is excited and probed in this case; it has a low frequency because the acoustic wavelength is much longer than the thickness of the film. The difference between the frequencies of the responses illustrates the possibility of quickly and unambiguously indentifying film delaminations with the transient grating technique.

trace, collected from a region of the sample that is tightly bound to the silicon substrate, reveals the lowest order Rayleigh mode, which has a velocity similar to the Rayleigh velocity of the substrate for this small *kh*. [The low frequency mode that is also observable in these data corresponds to an interfacial air mode. This oscillation disappears when the air is removed (34).] The difference in frequency between these two modes, which have the same wavelength, is large; it provides

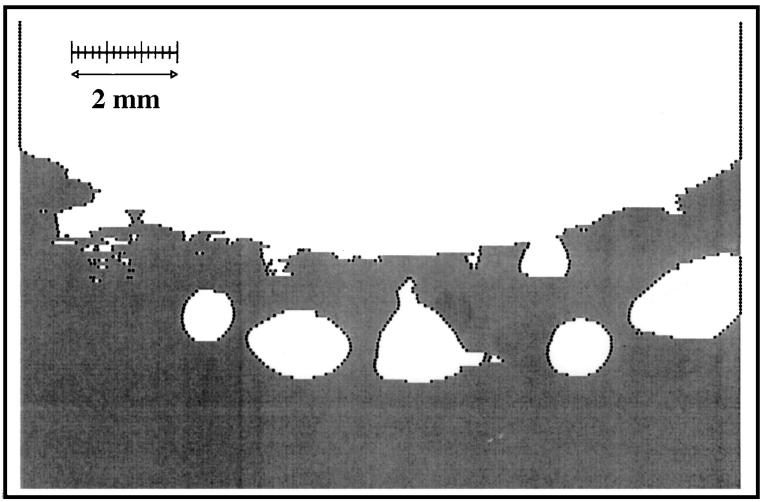

Figure 16 Map of adhesion in a sample that consists of a thin spin-cast polymer film bonded to a silicon wafer. The image was collected by recording acoustic frequencies as the sample was moved relative to the excitation and probing beams. The white and grey areas correspond to low- and high-frequency acoustic responses, respectively. The *top portion* of this image corresponds to a region of the sample where the silicon substrate was completely etched away. The *bottom portion* of the image corresponds to a region of the sample where the film is tightly bound to the silicon substrate. In between these two regions are locations where the film has delaminated from the substrate in an uncontrolled manner. To within the uncertainties of the measurement, we did not observe acoustic frequencies between the limits of the unsupported and tightly bound cases. The spatial resolution of the measurement is $\sim$50 μm.

an unmistakable signature for film delamination. Spatially scanning a sample that suffers from localized delaminations yields a map of the poorly adhering regions of the film, as shown in Figure 16. Note that this image shows only two response frequencies: those that correspond to values expected for a tightly bound film and those that are characteristic of complete delamination. It is natural to expect that in some limit of poor adhesion certain modes at certain wavevectors will exhibit frequencies between these two limits (33, 35). This area remains a subject of current research.

Measurements of Residual Stress Although the frequency of the lowest order Lamb mode measured in Figure 15 is small, it is larger than the value expected for an unstressed free-standing membrane with elastic properties typical of this type of polymer. The increase in frequency is caused by in-plane residual stresses that build up during thermal cure of the polymer film. These stresses are not released when a small region of the silicon support is removed. The stress most

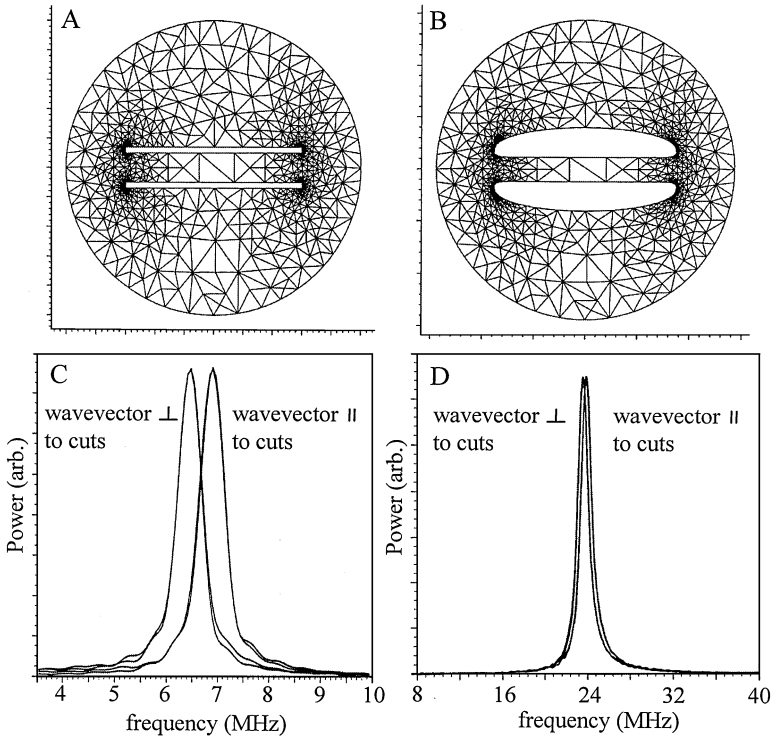

Figure 17 (*A*) and (*B*) show finite element modeling of a test structure designed to facilitate the measurement of residual stress in a thin polymer membrane formed by casting and curing a polymer against a silicon wafer and then etching the silicon away from a small circular region in the middle of the wafer. The test structure consists of two parallel slits cut in the membrane (*A*). These slits allow the stresses in the direction perpendicular to the cuts to relax to zero and stresses in the orthogonal direction to relax partially by an amount determined by the Poisson ratio (*B*). Measuring the frequency of acoustic modes excited in the strip of polymer between the slits highlights the effect of the stress. (*C*) and (*D*) show that the uniaxial stress distribution between the slits causes the frequency of the lowest order Lamb mode that propagates parallel to the cuts to be higher than the mode that propagates perpendicular to them. The difference in frequency can be used to determine the residual stress. As predicted by theory, this frequency difference decreases with increasing film thickness or acoustic wavevector [2.55 μm and 0.16 μm^{-1} for (*C*), and 7.29 μm and 0.23 μm^{-1} for (*D*)].

significantly affects the phase velocity of the lowest order Lamb mode at small *kh*; its influence can, in fact, exceed those of the elastic properties. This property allows the wavevector to be tuned for separate measurement of stress and elastic properties (34). Figure 17 illustrates data and a simple test structure that demonstrate this concept and unambiguously expose the effect of residual stress on the frequency of the lowest order Lamb mode. The structure, which was created by cutting

two parallel slits in a free-standing drumhead membrane formed by etching away a small circular region of the silicon wafer, features a uniaxial distribution of stress in the region between the slits. Comparison of the frequencies of acoustic modes excited with wavevectors parallel and perpendicular to the direction of stress demonstrates that the stress increases the phase velocity. This increase can be used to quantify the amount of stress. As expected by theory, and as illustrated in Figure 17, the magnitude of this shift decreases with increasing *kh*. When it is possible to measure the film at values of *kh* much less than 1, the stress can be determined directly, without the need for a test structure or precise knowledge of the elastic properties (34).

Elastic Moduli of Supported and Unsupported Films Although the data presented in the previous section were dominated by a single frequency, multiple acoustic modes are, in general, excited and probed with TG photoacoustics. The efficiency of exciting these modes and the strength with which they diffract light determine their relative contributions to the measured signal. Detailed calculations are typically required to compute these excitation and probing efficiencies (15, 36–40). In simple situations, it is possible to predict approximately the response without calculation. In an unsupported film, for example, one intuitively expects selective excitation of symmetric modes when weakly absorbed excitation pulses are used (19, 41). In that case, the stress pattern induced by spatially periodic heating is uniform throughout the depth of the film and does not effectively excite the anti-symmetric modes. Figure 18 presents data that confirm this expectation (19).

Measurements of multiple (or single) modes and their dispersion reveal the acoustic behavior of the waveguide and can be used to extract the elastic properties of the films. Analysis begins with measurements of acoustic frequencies at a range of acoustic wavelengths. Each frequency is then assigned a mode number either by calculation of the expected contributions of the various modes to the signal or, more commonly, by simple comparison of the dispersion characteristics with approximate anticipated behavior. The sum of squared differences between the measured dispersion and calculations that assume values for the physical properties of the waveguide provides a metric for the quality of the model. Adjusting these properties (e.g. elastic moduli, densities, and thicknesses) to optimize the quality of the fit yields the characteristics of the unknown components of the waveguide.

Figure 19*A* shows measurements and best fit calculations of dispersion in a set of polymer films [polyimide, DuPont PI2555, copolymer made from benzophenone-tetra-carboxylic dianhydride (BTDA) and oxydianiline, and BTDA and metaphenylenediamine] on silicon substrates (11, 38). The expected scaling of the dispersion with the product of the wavevector and the thickness confirms an aspect of the model of the waveguide, and demonstrates that the elastic moduli and densities of these films are not strongly dependent on their thickness in this range. The calculated dispersion captures all the features of the waveguide and, in this case, accurately determines the intrinsic acoustic properties (i.e. longitudinal and

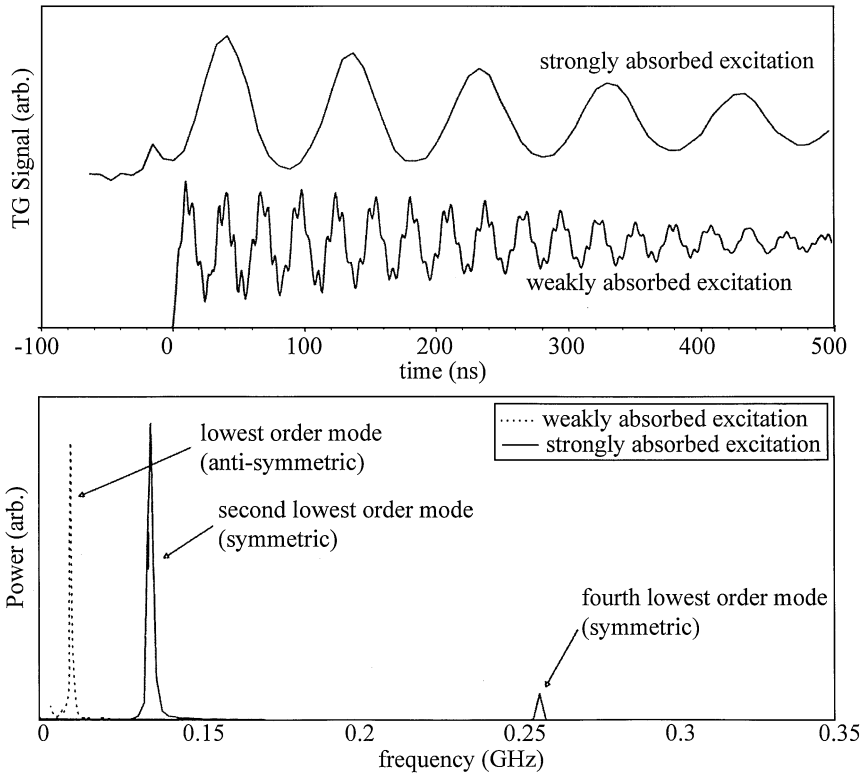

Figure 18 The *top frame* shows data collected by exciting a free-standing polymer film with crossed excitation pulses that are strongly or weakly absorbed by the polymer. The excitation in the weakly absorbing case is nearly uniform through the thickness of the film. This symmetric excitation couples only to symmetric Lamb modes of the unsupported thin film waveguide. The power spectra in the *bottom frame* reveal that the second and fourth lowest order Lamb modes (both symmetric) are excited. When the excitation light is strongly absorbed by the polymer, the excitation is not strongly symmetry selective. In this case the lowest order Lamb mode (anti-symmetric) is excited and probed most efficiently.

transverse velocities) of the films. Figure 19*B* shows acoustic dispersion measured in a single unsupported film of the same polymer used for the measurements shown in Figure 19*A* (19). Although even the qualitative characteristics of the dispersion of the unsupported film are, as expected, much different from those of the silicon-supported films, the fits in the two cases yield elastic moduli that agree to within experimental uncertainties.

An isotropic model of the waveguide accounts for the dispersion shown in Figure 19. This mechanical isotropy is consistent with other, nonmechanical, measurements (e.g. optical birefringence, differences between the in- and out-of-plane coefficients of thermal expansion) of these materials (42, 43). Other polymers

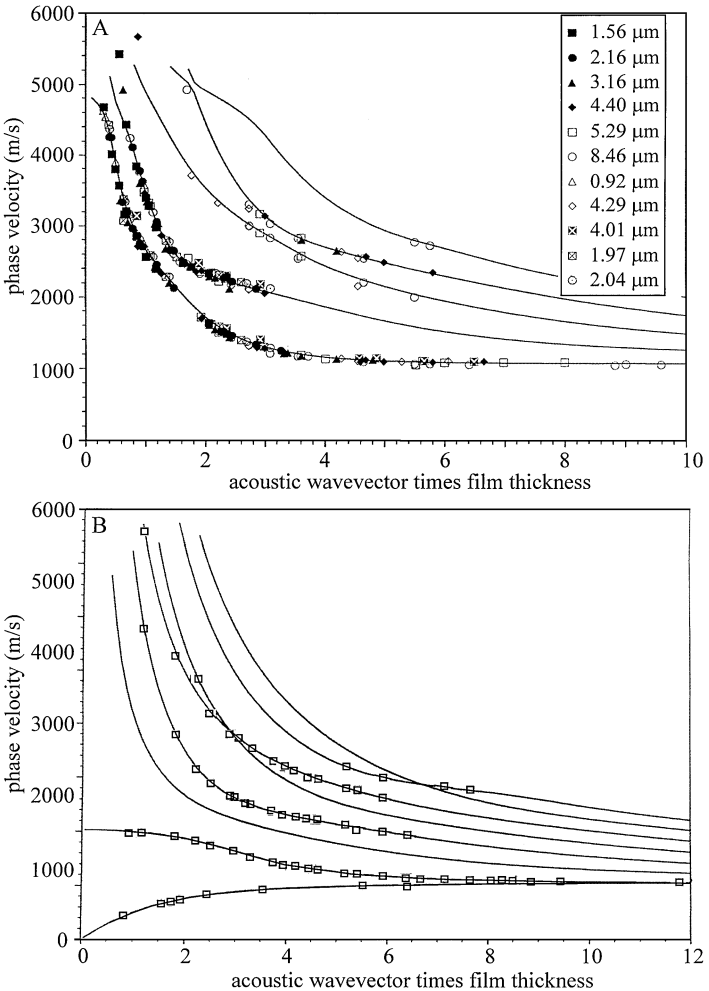

Figure 19 (*A*) shows measured (symbols) and best fit calculated (lines) acoustic dispersion in thin polymer films on silicon substrates. The expected scaling of the dispersion with the product of the film thickness (*h*) and the acoustic wavevector *(k)* was exploited to fit simultaneously a set of data collected at many acoustic wavevectors in samples with various thicknesses. The intrinsic longitudinal and transverse velocities of the film and its density were varied to fit (Marquardt-Levenberg, nonlinear least squares) the lowest two measured waveguide modes. (*B*) shows similar measured (symbols) and best fit calculated (lines) acoustic dispersion for a single sample of the same type of polymer film, but with the silicon substrate removed. The fit determines the intrinsic longitudinal and transverse velocities of the film. Although the dispersion in the silicon-supported and the -unsupported cases is quite different, the fitted isotropic mechanical properties are, to within experimental uncertainty, the same.

show pronounced ordering of chains in the plane of the film. This ordering leads to mechanical anisotropies that significantly affect the acoustics of waveguides formed with them. TG photoacoustics provides a remarkably convenient means to define, through measurements of acoustic dispersion, the degree of mechanical anisotropy in thin films. Figure 20 shows data and best fit computations (44) of the dispersion in unsupported polymer films (polyimide, DuPont PI2611, a polymer made from biphenyl-tetra-carboxylic dianhydride and *p*-phenylenediamine) that are known to exhibit high optical birefringence ($\Delta n \sim 0.2$) and a large anisotropy in the coefficients of thermal expansion (42, 43). The top frame shows the best fit isotropic model of the waveguide. This simple description clearly does not capture essential features of the measured dispersion. The bottom frame shows a fit that assumes the simplest symmetry that is consistent with other measurements: transverse isotropy (the in- and out-of-plane moduli can be different). The quality of the fit in this case is extremely good. The accuracy of the measurements and the uniqueness of the fit allow accurate determination of four of the five non-zero and unequal components in the stiffness tensor for these samples (44, 45).

Film Thickness For the analysis described above, the thicknesses of the films were determined using other techniques (e.g. stylus profilometry) and were not included as fitting parameters. It is not necessary, in general, to take this approach. Transient grating methods are, in fact, quite well suited for evaluating the thicknesses of transparent or opaque films in multilayer stacks (22, 46–48). This measurement exploits the strong dependence of the acoustic frequency on the thicknesses of the films. The elastic properties and densities of the layers may be known, or they may be determined at the same time as the thicknesses by using fitting techniques similar to those outlined in the previous section. The ability to measure precisely (repeatability $\sim$0.1 nm) the thickness of opaque thin films in a rapid ($\sim$1 s), noncontacting fashion with high spatial resolution represents a particularly attractive feature of TG methods for this application. Figure 21 shows the thickness of a layer of tungsten on titanium nitride on a silicon wafer measured using scanning electron micrographs (SEM) and transient grating photoacoustics at several points near the edge of the wafer (46, 47). In this region, the thickness of the tungsten increases gradually from zero at the very edge to a value that is maintained, to within a few percent, across the diameter of the wafer. The agreement between SEM and TG measurements validates the approach to determining film thickness. It is important to note here that SEM measurements of thickness are slow and require cleavage and, therefore, destruction of the sample. TG analysis is, on the other hand, fast and completely nondestructive.

Depth Profiling and Multilayer Analysis Samples with more than one film, such as the one analyzed in Figure 21, are often of interest. The physical modeling of multilayer structures or of films or substrates with depth-varying properties in most instances represents a straightforward extension of the formalism used for a single film. Although general statements about these complex systems are difficult, the

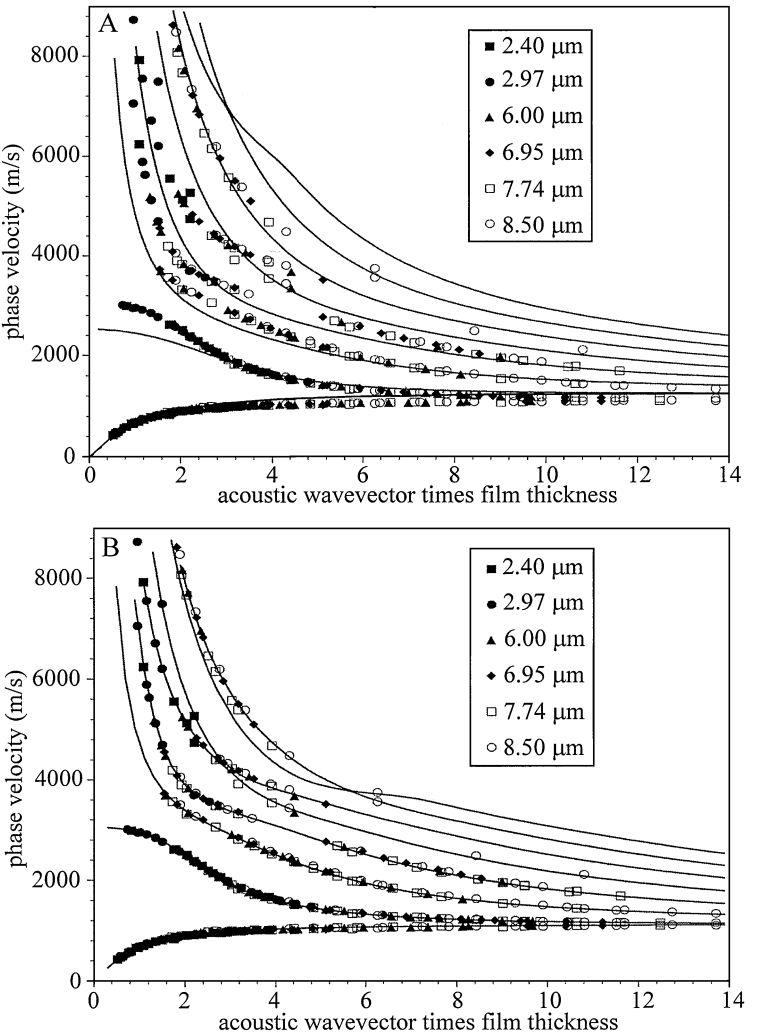

Figure 20 Measured (symbols) and best fit computed (lines) dispersion in unsupported polymer films that are known to exhibit preferential ordering of the polymer chains in the plane of the film. (*A*) shows best fit computations that use a simple isotropic model for the mechanical properties of the films. This model clearly does not account for the measured dispersion. (*B*) shows a fit computed using a model of the films that allows the in- and out-of-plane elastic properties to be different (i.e. transverse isotropic symmetry). The fit in this case agrees extremely well with measurements. (We note that our references 34, 44, 45 and 49 summmarized the elastic properties in terms of four acoustic velocities: in- and out-of-plane transverse and longitudinal speeds of sound. The in-plane transverse velocities in those cases were incorrectly defined in terms of the elastic constants c_{ij} and density ρ as $\sqrt{(c_{22} - c_{23})/(2\rho)}$. Although this quantity does not have a simple physical meaning, it can be used in a straightforward way with the correctly defined values of the other velocities and the density of the film to determine the elastic constants.)

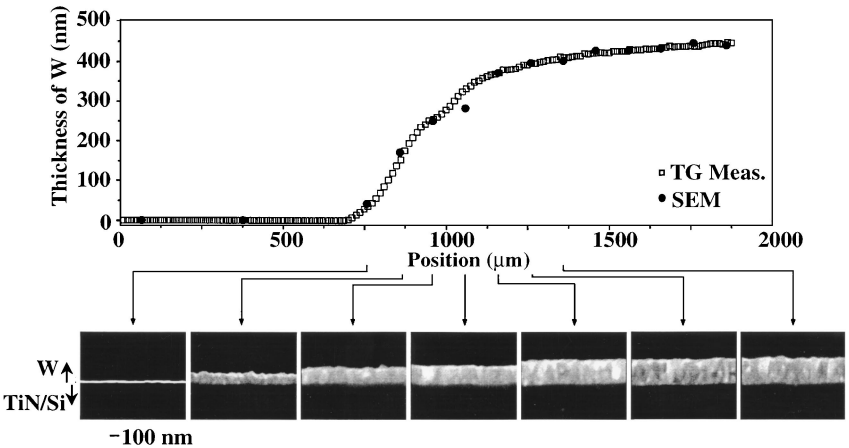

Figure 21 Thickness of a tungsten film at various positions near the edge of a 200-mm silicon wafer. The thicknesses were computed from acoustic frequencies measured at a single acoustic wavelength with excitation and probing beams focused to ∼50 μm spots on a wafer mounted on a translating stage. Measurements reveal the increase in thickness of tungsten beginning at an exclusion zone around the perimeter of the wafer. The measured thicknesses compare well with those determined from scanning electron micrographs collected from the edge of a cleaved (and therefore destroyed) wafer. Transient grating measurements enable nondestructive, noncontact, fast (∼1 s) determination of film thickness with angstrom-level precision.

dispersion can readily be used to evaluate elastic properties and thicknesses in these samples. (49–51) Figure 22 illustrates acoustic modes in unsupported polymer bilayers (49). Many simple features of the dispersion in single unsupported layers are absent from these systems. For example, the modes no longer have well defined symmetries, and the acoustic velocities fail to scale with the total thickness of the bilayer. Nevertheless, the measured acoustic dispersion can be inverted to determine the elastic properties of the layers (49).

Analysis of multilayer film stacks can be facilitated by the information obtained from bulk acoustic echoes measured on picosecond time scales (29). Figure 23 shows data obtained from a multilayer that represents a combination of metals common to integrated circuit technology. The somewhat complicated temporal response is determined by different sequences of acoustic reflections from interfaces; the measurements agree well with simulated results. Fitting this type of data to model calculations enhances the ability of TG methods to determine the thicknesses of many layers in complex multilayer stacks.

Structures with properties that vary continuously with depth represent an important class of materials that can also be analyzed. For these samples, gradually increasing the acoustic wavelength enables the elastic properties to be probed

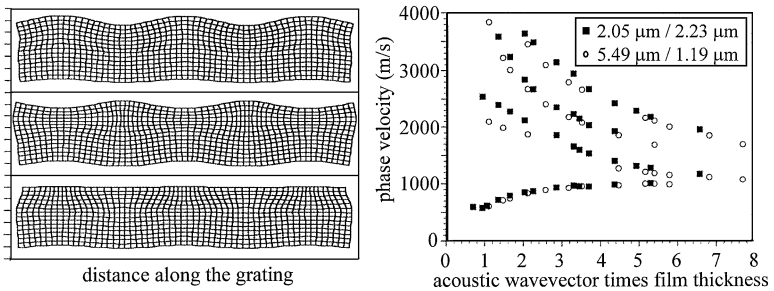

Figure 22 The frames on the *left* show grid distortion diagrams of the three lowest order acoustic waveguide modes in an unsupported film composed of two layers of polymer with different mechanical properties. The modes are affected by both of the polymers because the displacements extend throughout the bilayer. The well-defined anti-symmetric and symmetric nature of the modes in the simple single-layer system are absent from this structure. The waveguide properties of the bilayer film also do not simply scale with the product of the acoustic wavevector and the total thickness of the film. The frame on the *right* shows the measured dispersion in two bilayer films composed of different thicknesses of the two polymers. These data clearly demonstrate the absence of wavevector-thickness scaling. They also show that the various modes have different sensitivities to changes in the thickness of the two layers. Fitting the measured dispersion determines the elastic characteristics of the two layers.

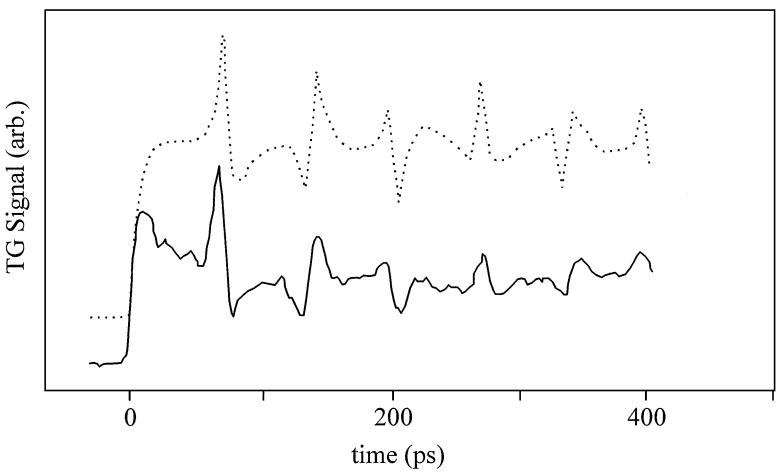

Figure 23 Transient grating photoacoustic data (solid line) from a multilayer of Al (100 nm) on TiW (75 nm) on a silicon susbtrate. The dashed line shows the simulated response. The features in the data correspond to reflections of longitudinal acoustic pulses that arrive back at the surface of the sample and change the intensity of diffracted probe light.

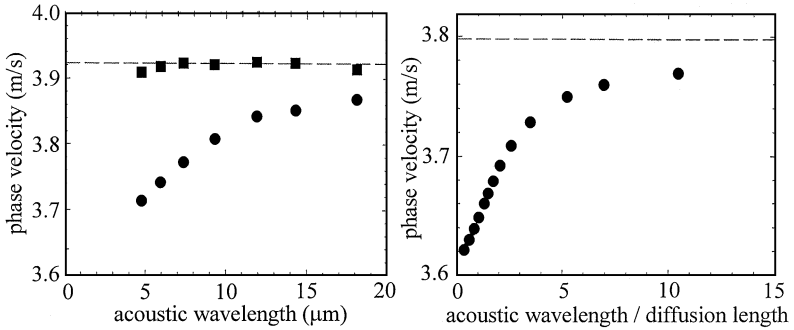

Figure 24 Measured (solid circles, *left frame*) and computed (solid circles, *right frame*) phase velocities for Rayleigh waves on a crystal of lithium niobate ($LiNbO_3$) that is doped with zinc. The local concentration of zinc is highest (∼5% Zn/Nb ratio) at the surface; it decreases to zero within a few microns into the depth of the crystal. As the acoustic wavelength increases, the Rayleigh mode probes deeper into the $LiNbO_3$, and the acoustic effects of the zinc diminish. The solid squares in the *left frame* correspond to measurements on an undoped substrate. The calculations on the *right* approximate the structure as a discrete system of 10 layers of material on a $LiNbO_3$ substrate. For simplicity, literature values for all of the elastic constants were assumed to decrease linearly with zinc concentration. The calculations capture the qualitative behavior of the measurements. The quantitative disagreement highlights shortcomings of the simple model and uncertainties in the values of the elastic and piezoelectric constants.

at progressively increasing depths into the bulk of the material. This strategy represents a form of surface acoustic depth profiling, and is illustrated in Figure 24. The sample in this case consists of a lithium niobate crystal with zinc thermally diffused from the surface of the substrate into its depth. The concentration of zinc decreases with depth on a length scale of a few microns. The measured acoustic effect of the zinc, which lowers the acoustic phase velocities, increases with decreasing acoustic wavelength. Computations that assume a linear decrease in all the components of the stiffness tensor of the lithium niobate with increasing zinc concentration and that treat the sample as a discrete multilayer stack with ten layers, capture the qualitative aspects of these depth profiling measurements (JE Graebner, G Kowach, L Dhar, JA Rogers & GW Kammlott, unpublished data).

ADDITIONAL TRANSIENT GRATING PHOTOACOUSTIC INVESTIGATIONS OF THIN FILMS

Analysis of Structures for Surface Acoustic Wave Filters

Measurement of structures for surface acoustic wave (SAW) filters and other devices that rely on high-frequency acoustic vibrations in thin films and multilayer stacks is an application perfectly suited for TG analysis. In a typical SAW device,

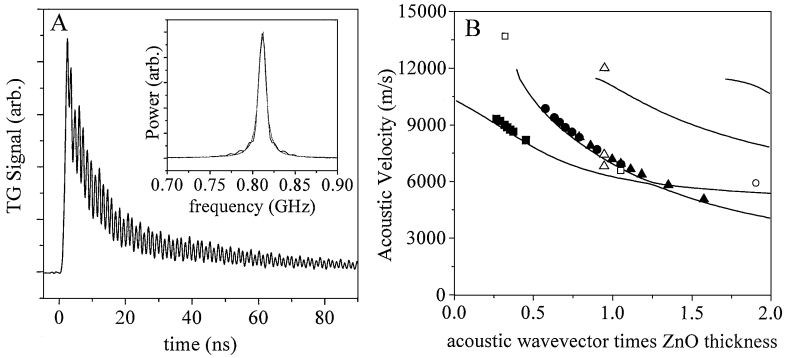

Figure 25 (*A*) shows transient grating data collected from a prototype structure for a high-frequency surface acoustic wave (SAW) filter: zinc oxide (∼1 μm)/platinum (∼100 nm)/ diamond (∼10 μm) /silicon substrate. A measurement at a single wavevector provides important insight into the behavior (e.g. frequency and quality factor) of a SAW filter that could be constructed with this combination of materials. Measurements at many wavevectors (solid symbols) (*B*) determine the dispersion of the structure, and reveal details of its acoustic behavior. The lines in (*B*) correspond to isotropic computations that use literature values (Voigt averages) of the elastic properties of the various layers. The open symbols are derived from operating frequencies of actual SAW filters constructed using this multilayer stack.

a piezoelectric film is stimulated electrically with interdigitated transducers (IDTs). Motion of this film launches acoustic modes that propagate along the surface of the structure until they are detected at another point by another IDT. The frequencies, damping rates, and velocities of the acoustic waveguide modes are of primary importance in these devices. These quantities can be simply and directly evaluated with TG photoacoustics (52; JA Rogers, GR Kowach & RL Willett, unpublished data). Figure 25 shows, for example, TG measurements of a multilayer stack designed for ultrahigh frequency SAW filter applications. It consists of a thin layer of zinc oxide (∼1 μm; piezoelectric), on a thin layer of platinum (∼100 nm), on a thick layer of diamond (∼15 μm), on a silicon wafer. The measurements determine, as usual, the acoustic phase velocities, damping rates, and dispersion. They compare well with the characteristics of actual SAW filters fabricated with these same samples.

In addition to acoustic properties, the piezoelectric constants of the films used for exciting the acoustic waves in SAW devices are important. Piezoelectricity couples physical displacements with electric fields. The acoustic frequencies are, as a result, sensitive to the magnitude of the piezoelectric effect. When the elastic constants are known, or when a sample can be measured with and without the piezoelectric effect present (by, for example, electrically shorting the surfaces of a thin film), then acoustic waveguide measurements provide insight into the piezoelectric characteristics of the sample (53). Figure 26 shows typical data from a

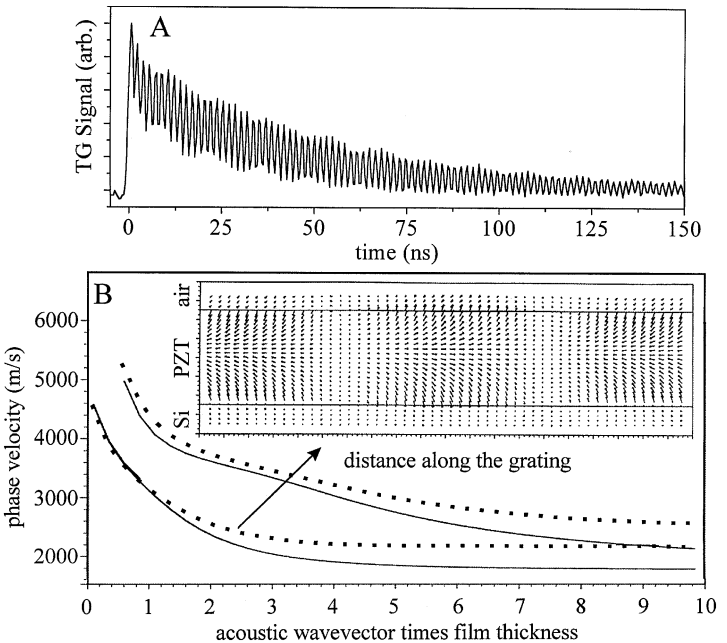

Figure 26 Data (*A*) and computed (*B*) dispersion for a piezoelectric (lead zirconium titanate—PZT) film on a silicon substrate. The excited modes in these cases involve coupled displacements and electric fields. The inset to (*B*) shows the electric field distribution for the lowest order waveguide mode at a wavevector-thickness product of 1.5. The degree of coupling, which is defined by the piezoelectric constants, affects the dispersion. The dashed lines in (*B*) were computed using literature values for the piezoelectric constants and mechanical properties of PZT. The solid lines use the same mechanical properties but take the piezoelectric constants to be zero. The sensitivity of the measured dispersion to the magnitudes of the piezoelectric constants makes their measurement possible with transient grating photoacoustic techniques.

thin film of the piezoelectric lead zirconium titanate. It also illustrates electric field distributions in the lowest order waveguide mode and the effect of piezoelectricity on the velocity and the dispersion.

Real-Time Measurement of Dynamic Changes in Thin Films

The relatively short time required for a TG measurement makes it possible to evaluate dynamic processes in thin films. The ability for remote evaluation is also important for this application. We illustrate two examples of this type of measurement. In the first, TG signal from a thin film of polyamic acid (formed from pyromelliticdianhydride and oxydianilline) spin cast onto a silicon wafer is monitored as the polymer thermally cures to a polyimide (54). Here, the excitation

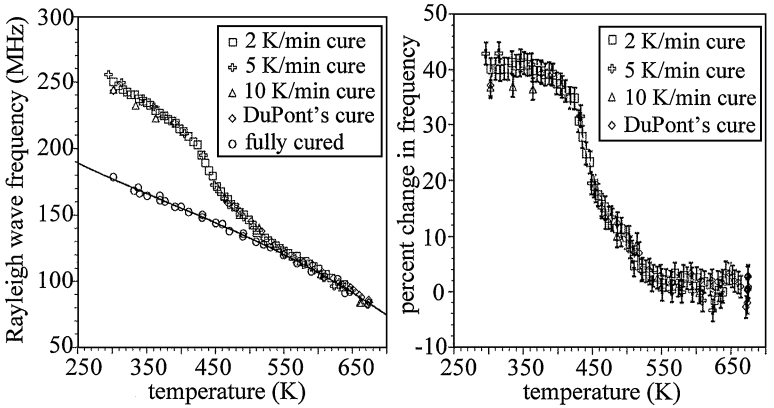

Figure 27 Evolution of the lowest order Rayleigh mode of a thin polymer film on a silicon substrate as it undergoes thermally induced cure. In these experiments the film was excited and probed by passing laser light through a transparent window in a vacuum chamber that contained the sample mounted on a heating block. Measurements were performed directly in real time during the cure, for various heating rates. The results demonstrate the ability to monitor film processing non-invasively with transient grating photoacoustics.

and probing beams pass through a window on a vacuum oven. Acoustic waves that are excited and probed during the reaction reveal the evolution of certain acoustic waveguide modes as the polyamic acid converts to polyimide, and as the resulting material cools back to room temperature. Figure 27 shows the evolution of the frequency of the lowest order waveguide mode, measured every 3 min during and after cure. The data indicate a relative insensitivity of the final acoustic frequency to the heating rate used for curing. These types of measurements can be useful for investigating the dynamics of cure and for process control in manufacturing settings.

Figure 28 illustrates another example of the use of TG methods to monitor time-dependent behavior of thin films. In this case, the lowest order waveguide mode of a film of copper on a silicon wafer is monitored as a function of time after deposition (MJ Banet & M Joffe, unpublished data). Slight changes are clearly observed; they are likely caused by annealing that is known to occur at room temperature in these materials. The dynamics of this process and its effect on the electrical characteristics of the copper are both extremely important for applications of this material in microelectronics.

Evaluation of Films for Microelectronics

There are many applications for TG photoacoustics that, like the one shown in Figure 28, exist in the area of microelectronics. We mention two here: evaluation

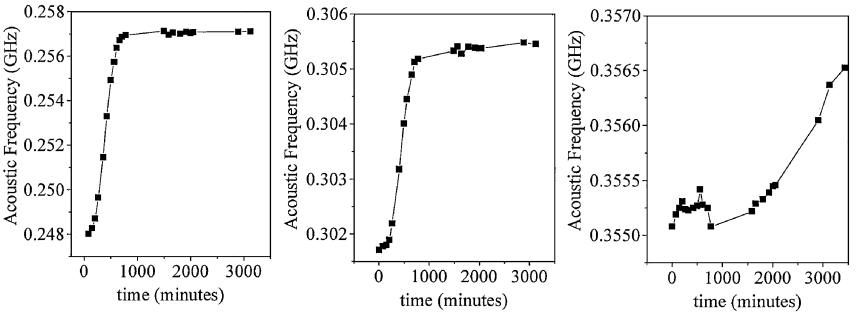

Figure 28 TG measurements of the acoustic frequency of the lowest order Rayleigh mode (wavelength 9.67 μm) on films of electroplated copper on silicon wafers. The data reveal a variation in the frequency with time after deposition of the copper. These changes are thought to be related to room-temperature annealing that is known to occur in electroplated copper films. These data show that the dynamics of the changes are functions of the thicknesses of the films: the frames on the *left*, *middle* and *right* contain data from films with nominal thicknesses of 3.02, 1.62 and 0.88 μm, respectively.

of elastic characteristics of nanoporous films of silica, and measurement of thicknesses of thin metal films. Inorganic and organic nanoporous films are primarily of interest for their possible use as low-dielectric constant interlayers, but they can also be used for thermal insulation and acoustic impedance matching layers. Because their fabrication is difficult to control and because many of their properties (e.g. the possibility and nature of diffusion of metal into the silica matrix) are unknown, techniques that can provide new information about these materials are important. Figure 29 shows typical TG data and dispersion measured in a $\sim$0.75 μm film of nanoporous silica, or nanoglass (55). The low density of the nanoglass ($\sim$65% porous in this case) and the large mismatch between its acoustic properties and those of the underlying silicon create pronounced waveguide dispersion. Fitting this dispersion allows accurate determination of the elastic properties of the thin film. For this sample, the measurements are consistent with mechanical isotropy; the fitted intrinsic acoustic velocities are similar to those in bulk samples of this material. It is interesting to note that higher order unguided or leaky modes can be accurately measured and modeled in this system.

Rapid, noncontact evaluation of the thicknesses of metal films used in microelectronics is now a well developed and extremely important application of TG or ISTS methods (22, 46–48). High-resolution maps of variations in the thickness of films of W, Cu, Al, Ti, Ta, and other materials deposited on wafers with diameters up to 300 mm is now routine and is fully commercialized and automated for process control applications (22). Evaluation of multilayer samples is also possible (22). Figure 30 displays some representative data (MJ Banet & M Fuchs, unpublished data).

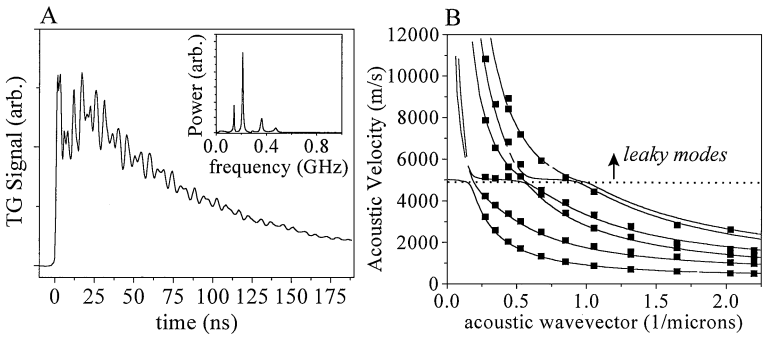

Figure 29 (*A*) shows transient grating data collected from a sample of aluminum (∼75 nm)/silica nanoglass (∼775 nm)/silicon substrate at an acoustic wavelength of 18.10 μm. The multiple frequencies correspond to several of the many acoustic waveguide modes that the structure supports at this wavelength. (*B*) shows the acoustic dispersion determined (symbols) in this structure by serial measurements similar to the one illustrated in (*A*), at various acoustic wavelengths. The rich and remarkable dispersion results partly from the extreme differences between the acoustic properties of the highly porous (∼65%) nanoglass and the silicon substrate. The multiple modes and the large variation in the phase velocities allow accurate characterization of the nanoglass, a material that is potentially important for low- dielectric constant layers in microelectronics.

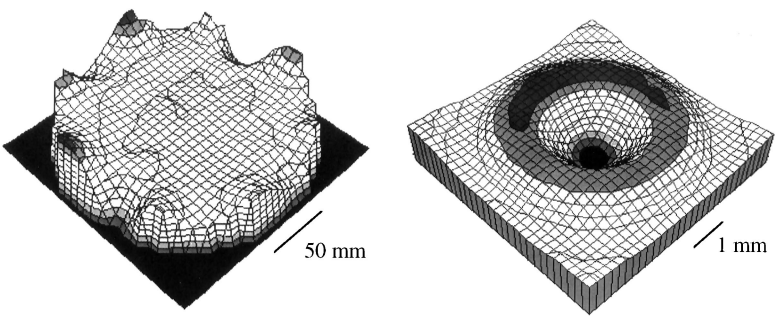

Figure 30 The frame on the *left* shows a full wafer map of the variations in thickness of a copper film electroplated onto a silicon wafer. The thickness varies from roughly 1200 to 1500 nm. The frame on the *right* shows a map of the variations in thickness near a defect caused by chemical mechanical polishing of the film. Here, the average thickness is ∼650 nm, and the total variation in thickness is ∼100 nm. The maps were recorded with a commercial ISTS-based instrument for thin film evaluation that uses miniaturized lasers and that requires no optical adjustments by the user.

EMERGING AND FUTURE APPLICATIONS

High Frequency Acoustics in Optical Fiber, Microcapillaries, and Microfluidic Systems

Although TG methods have primarily been applied to bulk or planar thin film systems, their use for exploring the physics of high-frequency acoustics in complex, three-dimensional microstructures represents an emerging direction that has potential relevance to microelectromechanical and microfluidic systems and to other areas of technological and scientific interest. The ability to rapidly map out the dispersion of these structures (whose physical dimensions can be comparable to the wavelengths of the stimulated acoustic modes) and to exploit heterodyne detection for measuring the typically small signals are two developments that enable these

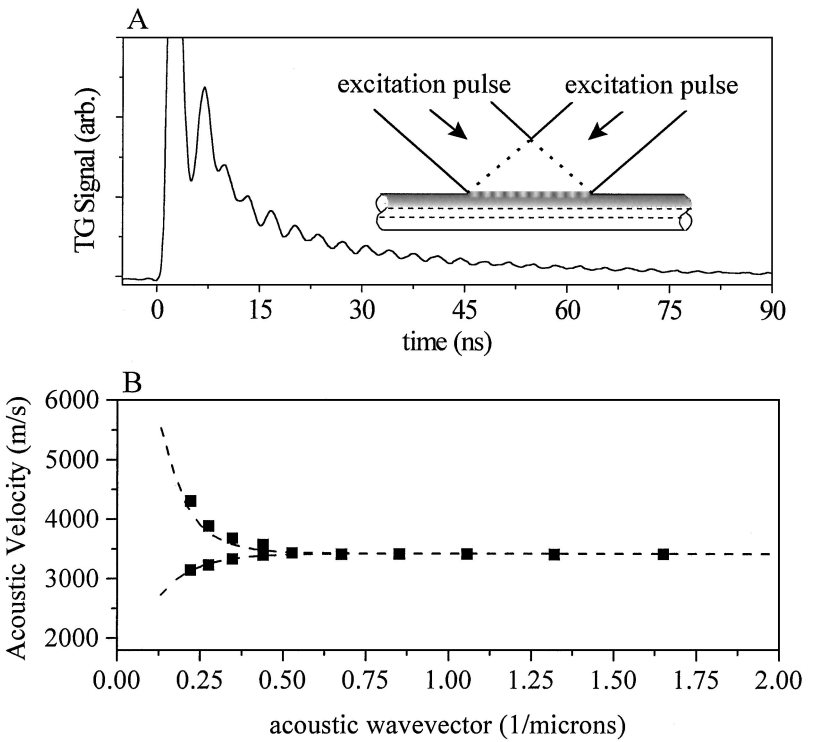

Figure 31 (*A*) schematically illustrates the geometry for using crossed picosecond laser pulses to excite axially propagating high-frequency acoustic modes of a cylinder. It also illustrates typical data collected from an optical fiber (diameter ~125 μm) with a thin metal coating. (*B*) shows the dispersion of acoustic modes of a hollow glass microcapillary tube (outer diameter ~140 μm, inner diameter ~96 μm) measured using an excitation geometry similar to that illustrated in (*A*). The dashed lines show the calculated dispersion of Lamb modes in a glass plate with a thickness equal to that of the walls of the microcapillary.

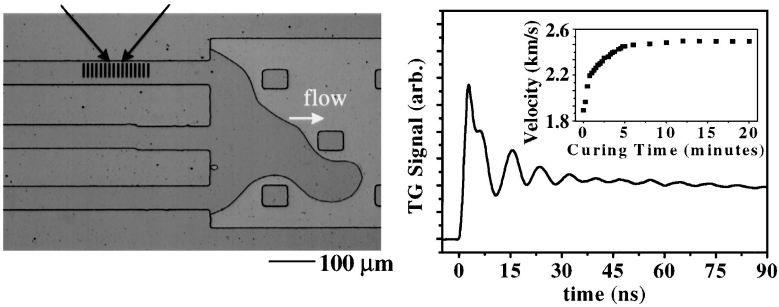

Figure 32 The image on the *left* shows an optical micrograph of a simple microfluidic system that consists of an array of channels formed by bonding a transparent embossed polymer against a silicon wafer coated with a thin layer of aluminum. Crossed excitation pulses that pass through the transparent polymer cause impulsive heating of the aluminum and the transparent liquid polymer that is housed in the channels. The frame on the *right* shows the time dependence of probe light diffracted by the motions excited in the microfluidic channel. The measured response is dominated by the Scholte-Stoneley mode of the liquid. It provides a simple and direct measurement of an intrinsic property (longitudinal acoustic velocity) of the ∼10 nanoliter volume of liquid that is probed. The inset shows the time evolution of the velocity of this mode as the liquid is photocured into a solid form.

applications. Optical fiber (∼120 μm diameter), cylindrical glass microcapillaries (∼140 and 96 μm inner and outer diameters, respectively), and planar microfluidic systems have recently been examined (56). Figure 31 shows data collected from an optical fiber and the measured dispersion of a hollow microcapillary tube. Figure 31 shows an optical micrograph of a simple planar microfluidic system. It also displays data collected from a ∼10 nL volume of polymer housed in one of the channels of the network. Monitoring the acoustic velocities provides a remote means for probing the mechanical properties of these tiny volumes of liquid. Figure 32 also illustrates the ability to measure, in real time, dynamic changes of the material. The capabilities demonstrated in Figures 31 and 32 may be useful for process monitoring and basic investigations of the mechanical properties of analyte in cylindrical capillary electrophoretic and chromatographic devices and in emerging planar microfluidic systems.

In-Plane Acoustic Echoes and Synthetic Phononic Bandgap Structures

In most TG experiments, the excited region of the sample is large compared with the characteristic propagation distance (defined by the group velocity and the attenuation) for the acoustic modes. In this regime, the measured decay of the acoustic component of the TG signal is exponential; it defines the intrinsic acoustic loss associated with the mode. If the excited region is small, or if there exist abrupt changes in the acoustic impedance in the plane of the sample, the propagating

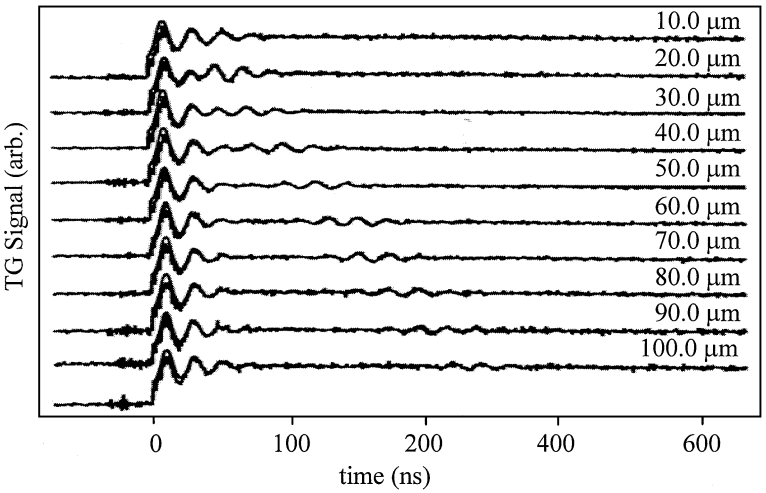

Figure 33 Measured and simulated data for acoustic and thermal disturbances excited near a subsurface flaw in a thin polymer film on a silicon substrate. Probe diffraction from the non-propagating thermal mode interferes with signal from the outgoing, counter-propagating surface acoustic pulses at times $<\sim$75 ns. At longer times, it is possible to observe the arrival of an acoustic pulse reflected from the flaw. Diffraction from this pulse interferes with the signal from the thermal mode and gives rise to oscillations at delays that correspond to the time required for the acoustic wave to travel from the excitation (and probing) region, to the flaw, and back to the probing region. As the distance between the excitation region and the flaw increases, the time for arrival of the echo also increases.

nature of the excited modes becomes apparent. This propagation can be exploited to detect buried flaws or other features that change locally the acoustic properties. Figure 33 shows a set of TG data and simulations for a signal that includes a thermal mode and an acoustic response that arises from the lowest order waveguide mode in a film on a substrate (51). The excited region is small and there is a subsurface void near, but spatially removed from, the excited region of the sample. The echo caused by reflection of the acoustic mode from the void clearly appears in the data; its time of arrival increases as the sample is translated to move the void away from the excitation and probing beams.

A regular array of these types of flaws or of other features that cause acoustic reflections forms an acoustic phononic crystal for guided modes. Figure 34 illustrates a one-dimensional crystal that consists of a microfabricated square-wave pattern of surface relief; this sample shows large phononic bandgaps that can be observed by exciting and monitoring acoustic waves directly in this structure with TG methods (57). These systems and TG characterization of them will, we believe, be important for the future of surface acoustic wave filters and other technologies that rely on guided acoustic motion in microstructures.

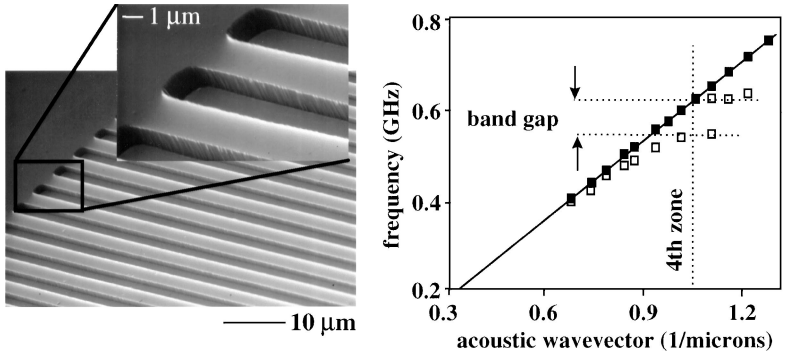

Figure 34 The *left frames* are scanning electron micrographs of a binary structure of relief on the surface of a substrate. The periodic change in acoustic impedance associated with this relief reflects Rayleigh waves. In fact, it forms a one-dimensional surface phononic crystal. The frame on the *right* shows the dispersion of a similar structure (open squares), as measured by using TG methods to excite and monitor acoustic waves directly in the crystal. The data show a large phononic bandgap at the fourth zone boundary. The solid squares correspond to data collected from a flat surface.

CONCLUSIONS

This review provides an overview of the physics and experimental techniques associated with transient grating, or impulsive-stimulated thermal scattering, acoustic measurements of thin films. Acoustic waveguide physics of layered structures provides a framework for interpreting the data; we demonstrated an accurate correspondence between TG measurements and acoustic waveguide computations in a diverse set of samples. We also illustrated (*a*) that it is possible to rapidly determine many important acoustic and mechanical properties, (*b*) that dynamic changes can be observed in real time, and (*c*) that complex microstructures can be evaluated. The experimental value of these methods derives from the rich range of information that TG measurements contain and from their applicability to a wide variety of technologically and scientifically interesting structures and materials. The commercial availability of low-cost diode pumped lasers that can be used for transient grating measurement will, we believe, make these techniques increasingly accessible and useful to researchers and engineers in many fields.

ACKNOWLEDGMENTS

We thank M Fuchs, M Joffe, and M Gostein of Philips Analytical; L Dhar, J Graebner, G Kowach, and R Willett of Bell Labs; and T Crimmins of M.I.T. for useful discussions and comments. The work at M.I.T. was supported in part by National Science Foundation grant no. DMR-9710140.

LITERATURE CITED

1. Pharr GM, Oliver WC. 1992. *MRS Bull.* 17:28–33
2. Schweitz J-A. 1992. *MRS Bull.* 17:34–45
3. Vinci RP, Vlassak JJ. 1996. *Annu. Rev. Mater. Sci.* 26:431–62
4. Thomsen C, Grahn HT, Maris JH, Tauc J. 1986. *Phys. Rev. B* 34:4129
5. Maris H. 1998. *Sci. Am.* 278:86
6. Eesley GL, Clemens BM, Paddock CA. 1987. *Appl. Phys. Lett.* 50:717
7. Wright OB, Kawashima K. 1991. *Phys. Rev. Lett.* 69:1668
8. Neubrand A, Hess P. 1992. *J. Appl. Phys.* 71:227
9. Hess P. 1996. *Appl. Surf. Sci.* 106:429
10. Duggal AR, Rogers JA, Rothschild M, Nelson KA. 1992. *Appl. Phys. Lett.* 60:692
11. Rogers JA. 1992. *Real time impulsive stimulated thermal scattering of thin polymer films.* MS thesis. MIT, Cambridge, MA. 165pp.
12. Meth JS, Marshall CD, Fayer MD. 1989. *Chem. Phys. Lett.* 162:306
13. Harata A, Nishimura H, Sawada T. 1990. *Appl. Phys. Lett.* 57:132
14. Kasinski JJ, Gomez-Jahn L, Leong KJ, Gracewski SM, Miller RJD. 1988. *Opt. Lett.* 13:710
15. Rogers JA, Nelson KA. 1994. *J. Appl. Phys.* 75:1534
16. Nizzoli F, Sandercock JR. 1990. In *Dynamical Properties of Solids,* ed. GK Horton, AA Maradudin. 6:285–335. Amsterdam: North-Holland
17. Marshall CD, Fishman IM, Dorfman RC, Eom CB, Fayer MD. 1992. *Phys. Rev.* B 45:10009
18. Kading OW, Skurk H, Maznev AA, Matthias E. 1995. *Appl. Phys.* A 61:253
19. Rogers JA, Yang Y, Nelson KA. 1994. *Appl. Phys. A* 58:523
20. Fayer MD. 1982. *Annu. Rev. Phys. Chem.* 33:63
21. Eichler HJ, Gunter P, Pohl DW. 1986. *Laser-Induced Dynamic Gratings.* New York: Springer
22. Gostein M, Bante M, Joffe M, Maznev A, Sacco R, et al. 1999. *Handbook of Silicon Semiconductor Metrology,* ed. AC Diebold. New York: Dekker. In press
23. Farnell GW, Adler EL. 1969. *Physical Acoustics, Principles and Methods,* ed. WP Mason, RN Thurston, pp. 109–66. New York: Academic
24. Viktorov IA. 1976. *Rayleigh and Lamb Waves.* New York: Plenum
25. Rogers JA. 1998. *J. Acoust. Soc. Am.* 104:2807
26. Rogers JA, Fuchs M, Banet MJ, Hanselman JB, Logan R, Nelson KA. 1997. *Appl. Phys. Lett.* 71:225
27. Maznev AA, Rogers JA, Nelson KA. 1998. *Opt. Lett.* 23:1319
28. Rogers JA, Nelson KA. 1996. *Physica B* 219–220:562
29. Crimmins TF, Maznev AA, Nelson KA. 1999. *Appl. Phys. Lett.* 74:1344
30. Maznev AA, Nelson KA, Yagi T. 1996. *Solid State Commun.* 100:807
31. Nalamwar AL, Epstein M. 1976. *J. Appl. Phys.* 47:43
32. Maznev AA, Akthakul A, Nelson KA 1999. *J. Appl. Phys.* 86:2818
33. Rogers JA, Nelson KA. 1995. *J. Adhes.* 50:1
34. Rogers JA, Nelson KA. 1995. *IEEE Trans. UFFC* 42:555
35. Rokhlin SI, ed. 1992. *J. Nondestr. Eval.: Special Issue on Modeling and Ultrasonic Characterization of Interfaces.* Vol. 11
36. Gusev V, Desmet C, Lauriks W, Glorieux C, Thoen J. 1996. *J. Acoust. Soc. Am.* 100:1514
37. Gracewski SM, Miller RJD. 1995. *J. Chem. Phys.* 103:1191

38. Duggal AR, Rogers JA, Nelson KA. 1992. *J. Appl. Phys.* 72:2823
39. Shen Q, Harata A, Sawada T. 1996. *Jpn. J. Appl. Phys.* 35:2339
40. Maznev AA, Akthakul A, Nelson KA. 1996. *J. Appl. Phys.* 86:2818
41. Meth JS, Marshall MD, Fayer MD. 1990. *J. Appl. Phys.* 67:3362
42. Noe SC, Pan JY, Senturia SD. 1992. *Polym. Eng. Sci.* 32:1015
43. Pottiger MT, Coburn JC, Edman JR. 1994. *J. Polym. Sci.B* 32:825
44. Rogers JA, Dhar L, Nelson KA. 1994. *Appl. Phys. Lett.* 65:312
45. Cocson JK, Hau CS, Lee PM, Poon CC, Zhong AH, et al. 1995. *Polymer* 36: 4069
46. Banet MJ, Fuchs M, Rogers JA, Reinold JH, Knecht JM, et al. 1998. *Appl. Phys. Lett.* 73:169
47. Banet MJ, Fuchs M, Belanger R, Hanselman JB, Rogers JA, Nelson KA. 1998. *Future Fab Int.* Jan.:297
48. Joffe MA, Gostein M, Maznev AA, Sacco R, Banet MJ. 1998. *Proc. 16th Int. VLSI Multilevel Interconnection Conf. (VMIC)*, Tampa, FL: Inst. Microelectronics Interconnection (IMIC) 1999.
49. Dhar L, Rogers JA, Nelson KA. 1995. *J. Appl. Phys.* 77:4431
50. Shen Q, Harata A, Sawada T. 1993. *Jpn. J. Appl. Phys.* 32:3628
51. Rogers JA. 1995. *Time-resolved photoacoustic and photothermal measurements on surfaces, thin films and multilayer assemblies.* PhD thesis. MIT, Cambridge, MA. 445 pp.
52. Du H, Zhu W, Graebner JE, Kammlott GW, Jin S, et al. 1999. *J. Appl. Phys.* 86:2220
53. Dhar L, Rogers JA, Nelson KA. 1994. *Ferroelectrics* 151:275
54. Rogers JA, Nelson KA. 1996. *J. Polym. Sci.B* 34:861
55. Rogers JA, Case C. 1999. *Appl. Phys. Lett.* 75:865
56. Rogers JA. 1999. *J. Appl. Phys.* 86:2959
57. Dhar L, Rogers JA. 2000 *Appl. Phys. Lett.* In press

Annual Review of Materials Science
Volume 30, 2000

CONTENTS

The Theory of Real Materials, *Marvin L. Cohen* 1
Tribochemical Polishing, *Viktor A. Muratov, Traugott E. Fischer* 27
High-Tc Superconductivity in Electron-Doped Layered Nitrides, *Shoji Yamanaka* 53
Holographic Polymer-Dispersed Liquid Crystals (H-PDLCs), *T. J. Bunning, L. V. Natarajan, V. P. Tondiglia, R. L. Sutherland* 83
Optical Generation and Characterization of Acoustic Waves in Thin Films: Fundamentals and Applications, *John A. Rogers, Alex A. Maznev, Matthew J. Banet, Keith A. Nelson* 117
Structure Evolution During Processing of Polycrystalline Films, *C. V. Thompson* 159
Mechanical Behavior of Metallic Foams, *L. J. Gibson* 191
Copper Metallization for High-Performance Silicon Technology, *R. Rosenberg, D. C. Edelstein, C.-K. Hu, K. P. Rodbell* 229
The Properties of Ferroelectric Films at Small Dimensions, *T. M. Shaw, S. Trolier-McKinstry, P. C. McIntyre* 263
IC-Compatible Polysilicon Surface Micromachining, *J. J. Sniegowski, M. P. de Boer* 299
SiGe Technology: Heteroepitaxy and High-Speed Microelectronics, *P. M. Mooney, J. O. Chu* 335
Ultrathin Diffusion Barriers/Liners for Gigascale Copper Metallization, *A. E. Kaloyeros, E. Eisenbraun* 363
Magnetocaloric Materials, *K. A. Gschneidner Jr., V. K. Pecharsky* 387
Advances in In Situ Ultra-High Vacuum Electron Microscopy: Growth of SiGe on Si, *Ruud M. Tromp, Frances M. Ross* 431
Layered Magnetic Manganites, *T. Kimura, Y. Tokura* 451
The Electronic Structure of Semiconductor Nanocrystals, *Al. L. Efros, M. Rosen* 475
Mechanisms for Enhanced Formation of the C45 Phase of Titanium Silicide Ultra-Large-Scale Integration Contacts, *J. M. E. Harper, C. Cabral Jr.,, C. Lavoie* 523
Synthesis and Characterization of Monodisperse Nanocrystals and Close-Packed Nanocrystal Assemblies, *C. B. Murray, C. R. Kagan, M. G. Bawendi* 545
Extremely High Density Longitudinal Magnetic Recording Media, *Dieter Weller, Mary F. Doerner* 611
Low Dielectric Constant Materials for ULSI Interconnects, *Michael Morgen, E. Todd Ryan, Jie-Hua Zhao, Chuan Hu, Taiheui Cho, Paul S. Ho* 645
Device Innovation and Material Challenges at the Limits of CMOS Technology, *P. M. Solomon* 681